Biogeosciences Discuss., https://doi.org/10.5194/bg-2019-32
Manuscript under review for journal Biogeosciences
Discussion started: 4 February 2019

Biogeosciences Discussions
Open Access
EGU

Benthic alkalinity and DIC fluxes in the Rhône River prodelta generated by decoupled aerobic and anaerobic processes

Jens Rassmann[a,1] , Eryn M. Eitel[b, 1], Cécile Cathalot[c], Christophe Brandily[c], Bruno Lansard[a] , Martial Taillefert[b] , Christophe Rabouille[a, 2]

[a] *Laboratoire des Sciences du Climat et de l'Environnement, LSCE/IPSL,CEA-CNRS-UVSQ-Université Paris Saclay, 91198 Gif-sur-Yvette, France*
[b] *School of Earth and Atmospheric Sciences; Georgia Institute of Technology, GA 30332-0340 Atlanta, USA*
[c] *IFREMER, Laboratoire Environnement Profond, 29280 Plouzané, France*

[1]Jens Rassmann and Eryn M. Eitel contributed equally to this article
[2] Corresponding author
Email adress: rabouill@lsce.ipsl.fr (Christophe Rabouille)
ORCID: https://orcid.org/0000-0003-1211-717X

1

Biogeosciences Discuss., https://doi.org/10.5194/bg-2019-32
Manuscript under review for journal Biogeosciences
Discussion started: 4 February 2019

Abstract

Estuarine regions are generally considered a net source of atmospheric CO_2 as a result of the high organic carbon (OC) mineralization rates in the water column and their sediments. Yet, the intensity of anaerobic respiration processes in the sediments tempered by the reoxidation of reduced metabolites controls the net production of alkalinity from sediments that may partially buffer the metabolic CO_2 generated by OC respiration. In this study, a benthic chamber was deployed in the Rhône River prodelta and the adjacent continental shelf (Gulf of Lions, NW Mediterranean) to assess the fluxes of total alkalinity (TA) and dissolved inorganic carbon (DIC) from the sediment. Concurrently, *in situ* O_2 and pH microprofiles, electrochemical profiles, pore water and solid composition were measured in surface sediments to identify the main biogeochemical processes controlling the net production of alkalinity in these sediments. The benthic fluxes of TA and DIC, ranging between 14 and 74 mmol m^{-2} d^{-1} and 18 and 78 mmol m^{-2} d^{-1}, respectively, were up to 8 times higher than the DOU fluxes (10.4 ± 0.9 mmol m^{-2} d^{-1}) close to the river mouth, but their intensity decreased offshore, as a result of the decline in OC inputs. Low nitrate concentrations and strong pore water sulfate gradients indicated that the majority of the TA and DIC was produced by sulfate and iron reduction. Despite the complete removal of sulfate from the pore waters, dissolved sulfide concentrations were low due to the precipitation and burial of iron sulfide minerals (12.5 mmol m^{-2} d^{-1} near the river mouth), while soluble organic-Fe(III) complexes were concurrently found throughout the sediment column. The presence of organic-Fe(III) complexes together with low sulfide concentrations and high sulfate consumption suggests a dynamic system driven by the variability of the organic and inorganic particulate input originating from the river. By preventing reduced substances from being reoxidized, the precipitation and burial of iron sulfide decouples the iron and sulfur cycles from oxygen, therefore allowing a flux of alkalinity out of the sediments. In these conditions, the sediment provides a source of alkalinity to the bottom waters which mitigates the effect of the benthic DIC flux on the carbonate chemistry of coastal waters.

Keywords

Carbon cycle; alkalinity flux; iron reduction; sulfate reduction; coupled element cycles

1. Introduction

As a link between continental and marine environments, the coastal ocean plays a key role in the global carbon cycle (Bauer et al., 2013). In particular, large fluxes of dissolved and particulate organic carbon (POC) are delivered by rivers to neighbouring continental shelves (Bianchi and Allison, 2009). In fact, even though shelf regions only occupy around 7 % of the global ocean surface area (Jahnke, 2010), they account for more than 40 % of POC burial in the oceans of which about half is buried in river deltas and estuaries (Hedges and Keil, 1995; McKee et al., 2004; Muller-Karger et al., 2005; Chen and Borges, 2009). River-dominated ocean margins receive substantial amounts of allochthonous and authigenic POC that settle to the sea floor (Rabouille et al., 2001; Burdige, 2005; Andersson et al., 2006), therefore increasing the organic carbon content of the sediments and enhancing mineralization rates (Canfield et al., 1993a; Mckee et al., 2004; Muller-Karger et al., 2005; Aller et al., 2008; Burdige, 2011). These processes allow estuarine and deltaic regions to constitute a net source of CO_2 to the atmosphere (Chen and Borges, 2009, Cai, 2011). In these river-dominated margins, high sedimentation rates of material containing large concentrations of POC decrease the residence time of organic carbon in the oxic sediment layers (Hartnett et al., 1998) and increase the relative contribution of anaerobic compared to aerobic degradation pathways of organic carbon (Canfield et al., 1993a). Anaerobic respiration processes, including denitrification, dissimilatory nitrate reduction to ammonium (DNRA), manganese reduction, iron reduction, and sulfate reduction create total alkalinity (TA) (Berner, 1970; Dickson, 1981; Wolf-Gladrow et al., 2007, Table 1) that increases the buffer capacity of pore waters (Ben-Yaakov, 1973; Soetaert et al., 2007), drives the carbonate saturation state of the pore waters towards oversaturation, and potentially trigger carbonate precipitation (Gaillard et al., 1989; Mucci et al., 2000; Jørgensen and Kasten, 2006; Soetaert et al., 2007; Burdige, 2011). In turn, the precipitation of carbonate species, such as calcite and aragonite,

Biogeosciences Discuss., https://doi.org/10.5194/bg-2019-32
Manuscript under review for journal Biogeosciences
Discussion started: 4 February 2019

consumes alkalinity within the sediments (Table 1, Eq. 1; Berner, 1970; Soetaert et al., 2007; Krumins et al., 2013; Brenner et al., 2016). Anaerobically produced alkalinity may also be consumed close to the sediment-water interface (SWI) by the aerobic reoxidation of reduced species such as NH_4^+, Mn^{2+}, Fe^{2+}, and dissolved sulfide (Table 1, Eq. 2-4; Jourabchi et al., 2005; Krumins et al., 2013; Brenner et al., 2016). However, the precipitation and ultimate burial of iron sulfide minerals may prevent reoxidation of dissolved sulfide and Fe^{2+} and result in the net production of alkalinity in sediments. Thus, the net TA flux across the SWI depends on the type and intensity of anerobic respiration, on carbonate precipitation/dissolution and whether reduced species are reoxidized by dissolved oxygen after diffusion upwards or trapped in anaerobic sediment layers by precipitation (Hu and Cai, 2011a; Krumins et al., 2013; Łukawska-Matuszewska et al., 2018).

To characterize the biogeochemical conditions in which sediments provide an alkalinity source to coastal waters, it is crucial to relate this reaction network to net benthic fluxes of alkalinity and dissolved inorganic carbon (DIC) measured *in situ*. A high ratio (> 1) of benthic TA to DIC fluxes would increase the buffer capacity of the bottom waters. This could influence the coastal carbon cycle by increasing the storage capacity of CO_2 in coastal waters over long time scales (Thomas et al., 2009; Andersson et al., 2012; Brenner et al., 2016). The objectives of this study were to investigate if sediments from deltaic regions exposed to large riverine inputs of carbon and minerals represent an alkalinity source to the bottom waters and identify the biogeochemical processes responsible for the net production of alkalinity in these sediments. To achieve these objectives, TA and DIC benthic fluxes, dissolved oxygen uptake (DOU) fluxes, burial fluxes of reduced substances and the main biogeochemical processes involved in organic carbon mineralization in sediments were determined along a gradient of organic carbon and mineral inputs to the sea floor in the Rhône River delta (France).

Biogeosciences Discuss., https://doi.org/10.5194/bg-2019-32
Manuscript under review for journal Biogeosciences
Discussion started: 4 February 2019

2. Study site and methods

2.1 The Rhône River delta

The Rhône River subaqueous delta, also called prodelta due to its prograding characteristics, is a wave-dominated delta located in the Gulf of Lions (France), a microtidal continental margin. The Rhône River is the main source of freshwater, sediments (including iron oxides), and POC to the Mediterranean Sea (Sempéré et al., 2000). The river plume is generally oriented southwestward due to the combined effects of wind forcing and the Coriolis effect (Estournel et al., 1997). The Grand Rhône River mouth is characterized by a prodeltaic lobe (Got et al., 1990) that can be divided into three main areas based on bathymetry and sedimentation rates: the proximal domain within a 2 km radius of the river outlet and with water depths between 10 and 30 m; the prodelta domain between 2 and 5 km with water depths ranging from 30 to 70 m; and the distal domain further offshore with water depths greater than 70 m. The sediments of the three domains are characterized by a strong biogeochemical gradient from the Rhône River mouth to the Gulf of Lions continental slope (Lansard et al., 2009).

Most of the riverine particles settle in the vicinity of the river mouth leading to mean apparent accumulation rates of up to 37-48 cm yr^{-1} (Charmasson et al., 1988), including about 80 % of the particles deposited during flood events (Maillet et al., 2006; Cathalot et al., 2010). Thus, sediments from the proximal domain are dominated by the periodic accumulation of terrestrial organic-rich particles (Radakovich et al., 1999; Roussiez et al., 2005). Offshore, sedimentation rates decrease rapidly and reach typical values for shelf regions (< 0.1 cm yr^{-1}), in the distal domain (Miralles et al., 2005). The sediments in all the study area are fine grained and of cohesive nature (Roussiez et al., 2005). Their total organic carbon content is higher than 2 % close to the river mouth and decreases offshore (Lansard et al., 2008). The sedimentary inorganic carbon content ranges between 28 and 38 % (Roussiez et al., 2005) and is mostly composed of calcite and magnesian calcite (Rassmann et al., 2016). Sediment respiration rates are high in the proximal domain and decrease offshore (Lansard

et al., 2009; Pastor et al., 2011; Cathalot et al., 2013; Rassmann et al., 2016). These sediments are characterized by strong anaerobic production of TA and DIC (Rassmann et al., 2016), but whether this alkalinity is consumed in the oxic sediment layer or released to the bottom waters has yet to be determined.

2.2 Bottom water sampling and analyses

The AMOR-B-Flux cruise took place on-board the RV Tethys II (CNRS-INSU) in September 2015. The investigated stations were located in the river plume along a nearshore-offshore transect (Fig. 1 and Table 2). Bottom water samples were collected with 12-L Niskin® bottles as close as possible to the sea floor. The seawater temperature was measured using a thermometer with a precision of 0.1 °C and the salinity with a conductivity based thermosalinometer with a precision of 0.1. Triplicate pH measurements, reported on the total proton scale (pH_T), were carried out within 1 hour after sampling by spectrophotometry with unpurified m-cresol purple as indicator dye (Clayton and Byrne, 1993) and a precision of ± 0.01 pH units. Dissolved oxygen concentrations were analysed by Winkler titration (Grasshoff et al., 1983) within twelve hours after sampling with a precision of ± 0.5 µM.

2.3 In situ benthic chamber deployments

Benthic fluxes and sediment depth profiles of the main redox species involved in the remineralization of organic carbon were determined with an autonomous benthic lander (Jahnke et and Christiansen, 1989). The lander was equipped with a single benthic chamber, water syringe sampling system, and retrofitted with a programmable, battery-powered ISEA IV In Situ Electrochemical Analyzer and a SUBMAN-1 in situ micromanipulator from Analytical Instrument Systems, Inc. (AIS, Inc.) to simultaneously obtain depth profiles of redox chemical species with mercury/gold (Hg/Au) amalgam voltammetric microelectrodes (Luther et al., 2008; Tercier-Waeber and Taillefert, 2008). The chamber encloses a 30 x 30 cm sediment surface area with a certain volume

Biogeosciences Discuss., https://doi.org/10.5194/bg-2019-32
Manuscript under review for journal Biogeosciences
Discussion started: 4 February 2019

of overlying water determined by measuring the concentration of two tracers (iodide and bromide) injected immediately after closure of the chamber. Homogenization of the overlying waters was assured with a stirrer integrated in the chamber lid. TA and DIC concentrations were determined in the benthic chamber water samples collected as a function of time. The slopes of the concentration-time plots were estimated using a restricted maximum likelihood estimator (REML) that takes uncertainties of individual measurements into account. Finally, benthic fluxes across the SWI (F_i) were calculated from the slopes of these concentration-time-plots and the chamber height (Eq. 1),

$$F_i = H \cdot \frac{dC_i}{dt} \quad (1)$$

where H is the overlying water height in the benthic chamber, C_i represents the concentration of the analyte i (TA or DIC), and t is time.

2.4 In situ microprofiling of dissolved oxygen and pH

A separate benthic lander, carrying a benthic microprofiler (Unisense®), was deployed to measure *in situ* microprofiles of dissolved oxygen and pH (Cai and Reimers, 1993; Rabouille et al., 2003, Rassmann et al., 2016 and references therein). Up to five oxygen and two pH microelectrodes were simultaneously deployed, and vertical depth profiles were measured with a 200 µm resolution. As their response to variations in oxygen concentrations is linear, the O_2 microelectrodes were calibrated with a two-point calibration technique using the bottom water O_2 concentration determined by Winkler titration and the anoxic pore waters. The pH microelectrodes were calibrated using NBS buffers (pH 4.00, 7.00 and 9.00 at 20°C) and the spectrophotometrically determined pH of the bottom waters was used to correct for the difference in the liquid junction potential between seawater and the NBS buffers. Signal drift of O_2 and pH microelectrodes during profiling was checked to be less than 5 %.

Biogeosciences Discuss., https://doi.org/10.5194/bg-2019-32
Manuscript under review for journal Biogeosciences
Discussion started: 4 February 2019

2.5 Sediment sampling, porosity measurements, and ex situ voltammetric profiling

At each sampling station, sediment cores were collected using an UWITEC® single corer (length 60 cm, inner diameter 9 cm) within 30 m from the site where the landers were deployed and processed within 30 minutes after collection. Sediment porosity profiles were determined by slicing one of the cores with a 2 mm resolution until 10 mm depth, a 5 mm resolution until 60 mm, and a 10 mm resolution down to the bottom of the cores. Porosity was calculated from the bottom water salinity, an average sediment density of 2.65 g cm^{-3} and the weight difference between the wet and dried sediment after one week at 60 °C.

Ex situ voltammetric profiles were obtained in a separate core with a AIS, Inc. DLK-70 potentiostat in a three electrode configuration, including Hg/Au working microelectrode constructed from Pyrex glass pulled to a tip of 0.4 mm diameter to minimize particle entrainment during the profiles (Luther et al., 2008), an Ag/AgCl reference electrode, and a platinum counter electrode. The Hg/Au voltammetric electrode was deployed in the sediment using a DLK MAN-1 micromanipulator (AIS, Inc). Using a combination of linear sweep and anodic and cathodic square wave voltammetry, Hg/Au voltammetric microelectrodes are able to simultaneous quantify dissolved O_2, Mn^{2+}, Fe^{2+}, total dissolved sulfide ($\Sigma H_2S = H_2S + HS^- + S^0 + S_x^{2-}$), as well as organic complexes of Fe(III) (org-Fe(III)) and iron sulfide clusters (FeS_{aq}), which are not quantifiable but reported in normalized current intensities (Tercier-Waeber and Taillefert, 2008). Hg/Au microelectrodes were calibrated for dissolved O_2 using *in situ* temperature and salinity of the overlying waters to determine the dissolved O_2 concentrations at saturation (Luther et al., 2008). They were also calibrated externally with $MnCl_2$ to quantify all other species according to the pilot ion method (Luther et al., 2008). All voltammetric data was integrated using VOLTINT, a semiautomated Matlab® script with peak recognition software (Bristow and Taillefert, 2008).

Biogeosciences Discuss., https://doi.org/10.5194/bg-2019-32
Manuscript under review for journal Biogeosciences
Discussion started: 4 February 2019

2.6 Pore water and solid phase extractions and analyses

Sediment pore waters were extracted using rhizon filters with a mean pore size of 0.1 µm (Seeberg-Elverfeldt et al., 2005) in a glove bag that was extensively flushed with N_2 to create an anaerobic atmosphere. Pore waters were analyzed immediately onboard for dissolved phosphate concentrations using the paramolybdate method (Murphy and Riley, 1962) as well as for dissolved Fe^{2+} and total dissolved iron concentrations using the ferrozine method (Stookey, 1970). Pore water and bottom water fractions were poisoned with $HgCl_2$ for TA and DIC, acidified for sulfate, and stored at 4 °C until analysis in the laboratory. Total alkalinity was measured by open cell titration with 0.01 M HCl (Dickson et al., 2007). DIC concentrations were analyzed with a DIC analyzer (Apollo/SciTech®) on 1 ml samples as previously described (Rassmann et al., 2016). The TA and DIC methods were calibrated using certified reference materials for oceanic CO_2 measurements provided by the Scripps Institution of Oceanography (batch n°136). The relative uncertainty for both DIC and TA was ± 0.5 % of the final value. Sulfate concentrations were quantified after dilution by ion chromatography on an ICS 1000 chromatograph (Dionex) with an IonPac AS 9 HC column and AG 9 HC guard by suppressed conductivity with an AERS 500 suppressor (ThermoFisher Scientific). A 9 mM solution of Na_2CO_3, at a flow rate of 1 ml min^{-1} was used as the eluent. The relative uncertainty of this method was ± 1.6 %. Separate pore water fractions were frozen at -18 °C for sulfate analysis by high performance liquid chromatography using a Waters, Inc. 1525 binary pump with Waters 2487 absorbance detector at 215 nm and a Metrohm Metrosep A Supp 5 anion exchange column (150 mm x 4.0 mm) with a 1.0 mM $NaHCO_3$ / 3.2 mM Na_2CO_3 eluent at a flow rate of 0.7 ml min^{-1} (Beckler et al., 2014). To measure ammonium (NH^+_4) concentrations, samples were diluted and analysed using the indophenol blue method (Grasshof et al., 1983). The uncertainty of the method was about 5 %. Pore water fractions were also acidified with 2 % HCl for Ca^{2+} analysis by inductively-coupled plasma atomic emission spectroscopy (Ultima 2, Horiba Scientific). The method was validated with mono-elemental standards and standard solutions (IAPSO, CASS-4, and NASS-6 seawater reference materials) and displayed an external relative uncertainty of ± 2-3 % depending on the sample series.

Close to the Rhône River mouth, at station A, Z, and AK, one core was subsampled from the side with 1cm diameter corers made of cut 10-ml syringes every 5 cm through pre-drilled holes. The content of these subsamples was carefully inserted in gas tight vials containing deionized water and $HgCl_2$ solution and kept at 4°C until methane analysis. Dissolved methane was quantified after degassing of the pore waters into the headspace and quantified by gas chromatography with a relative uncertainty of ± 5 % (Sarradin and Caprais, 1996). The position of the sulfate-methane transition zone (SMTZ) was determined as the zone around the depth where $[SO_4^{2-}] = [CH_4]$ (Komada et al., 2016). Finally, acid volatile sulfur (AVS) for the determination of FeS_s was extracted from the same sediment used for the pore water extractions and conducted in triplicate by cold acid distillation of H_2S (g) under anoxic conditions that was trapped by NaOH and quantified voltammetrically (Henneke et al., 1991).

2.7 Nanoparticulate FeS and ion activity product for FeS precipitation

As a significant fraction of FeS nanoparticles may pass through the rhizon filters (0.1µm) used to extract pore waters (Nakayama et al., 2016) and the ferrozine method is well known to dissolve FeS nanoparticles (Davison et al., 1998), the difference between spectrophotometrically-determined Fe^{2+} concentrations ($[\Sigma Fe^{2+}]_{FR}$) and electrochemically-determined Fe^{2+} concentrations ($[Fe^{2+}_{echem}]$) in the pore waters was attributed to FeS nanoparticles (FeS_0), as demonstrated previously (Bura-Nakic et al., 2009; Eq. 2).

$$[FeS_0] = [\sum Fe^{2+}]_{FR} - [Fe^{2+}_{echem}] \quad (2)$$

In this interpretation, FeS_0 nanoparticles encompass both the molecular clusters of FeS (FeS_{aq}) detected electrochemically, which must be smaller than 5 nm in diameter to diffuse to the electrode (Buffle, 1988), and the larger FeS nanoparticles that are not detected voltammetrically. The ionic activity product (IAP) for the precipitation of FeS was calculated using Eq. 3 (Beckler et al., 2016),

$$pIAP = \log\left(\frac{\gamma_{Fe(II)}[Fe^{2+}]\gamma_{\mathrm{HS}}\alpha_{\mathrm{HS}}\Sigma H_2S}{\{H^+\}}\right) \quad (3)$$

Biogeosciences Discuss., https://doi.org/10.5194/bg-2019-32
Manuscript under review for journal Biogeosciences
Discussion started: 4 February 2019

where $\gamma_{Fe(II)}$ and γ_{HS} represent the activity coefficients of Fe^{2+} and HS^{--}, $\alpha_{HS} = \frac{\{H^+\}K_{a1}}{\{H^+\}^2+\{H^+\}K_{a1}+K_{a1}K_{a2}}$ is calculated with the acid dissociation constant of H_2S ($K_{a1} = 10^{-6.88}$) and HS^- ($K_{a2} = 10^{-17}$) (Davison, 1991), and $\{H^+\}$ is the activity of the proton. Activity coefficients of Fe^{2+} (Millero and Schreiber, 1982) and HS^- (Millero, 1983) were calculated using Pitzer parameters.

2.8 Calculations of oxygen uptake and AVS burial rates

Diffusive oxygen uptake (DOU) fluxes were calculated using Fick's first law (Berner, 1980, Eq. 4),

$$DOU = -\emptyset \cdot D_s \cdot \frac{d[O_2]}{dz}\Big|_{z=0} \tag{4}$$

where ϕ is the sediment porosity, D_s is the apparent diffusion coefficient in the sediments, and $\frac{d[O_2]}{dz}\Big|_{z=0}$ is the oxygen gradient at the SWI. The D_s coefficients were adjusted for diffusion in a porous environment according to: $D_s = \frac{D_0}{(1+3\cdot(1-\emptyset))}$ with the diffusion coefficient in free water (D_0) chosen according to Broecker and Peng (1974) and recalculated to *in situ* temperature by the Stokes-Einstein relation (Li and Gregory, 1974).

AVS burial fluxes were estimated using available sedimentation rates (ω from Charmasson et al. (1998) and Miralles et al. (2005)), average AVS concentrations and porosities of each sediment core, according to Eq. 5,

$$AVS_{burial} = (1-\emptyset) \cdot \omega \cdot AVS \cdot \rho \tag{5}$$

where ϕ is the sediment porosity, ω the sedimentation rate, and ρ the sediment dry bulk density.

2.9 Stoichiometric ratios

To determine the relationship between net TA and DIC production and to establish whether sulfate reduction represents the main source of TA and DIC in these sediments, stoichiometric ratios of the relative production of TA compared to DIC (r_{AD}), as well as TA (r_{AS}) and DIC (r_{DS}) compared to sulfate consumption, were calculated from the pore water data and compared to theoretical ratios

from the reaction stoichiometries (Table 1). Experimental stoichiometric ratios were obtained from the slope and standard deviation of the linear regression of TA, DIC, and sulfate property-property plots of concentration changes with respect to bottom water concentrations at each depth in the pore waters (ΔTA, ΔDIC and ΔSO_4^{2-}) relative to each other after correcting for differences in TA, DIC and sulfate diffusion in the sediments (Berner, 1980, Eq. 6),

$$r_{ij} = \frac{D_i \cdot \Delta i}{D_j \cdot \Delta j} \quad (6)$$

where i is the concentration of either TA or DIC, j the concentration of SO_4^{2-} or DIC and D_i and D_j are the corresponding diffusion coefficients. At the pH of the pore waters (pH ~ 7.5), more than 95 % of DIC and carbonate alkalinity are composed of bicarbonate ion (HCO_3^-). Given the relatively small difference in the diffusion coefficients of HCO_3^- and CO_3^{2-} (11.8 and 9.55 x 10^{-6} cm^2 s^{-1} at 25°C, Li and Gregory, 1974) and the high proportion of HCO_3^- relative to CO_3^{2-}, the diffusion coefficient of HCO_3^- was adopted for both TA and DIC diffusion.

The effect of the precipitation or dissolution of calcium carbonate on TA and DIC variations was also accounted for by considering the Ca^{2+} concentration gradients in the pore waters. For these calculations, the absolute value of the Ca^{2+} concentration relative to its bottom water concentration (ΔCa^{2+}) was added to the ΔTA or ΔDIC after taking the corresponding diffusion coefficients into account ($D_{TA}\Delta$ TA + $2D_{Ca}|\Delta Ca^{2+}|$ for alkalinity and $D_{DIC}\Delta$ DIC + $D_{Ca}|\Delta Ca^{2+}|$ for DIC) and plotted against $D_{SO42-}\Delta SO_4^{2-}$. The calculated slope provided a stoichiometric ratio corrected for the precipitation of calcium carbonate (r_{IJc}). Pore water saturation states, regarding Calcite (Ω_{Ca}), were calculated according to the equation proposed by Mucci (1983) and Millero (1995).

3.Results

3.1 Bottom water and surface sediment characteristics

At all stations, bottom water salinities ranged from 37.5 to 38.0 and temperatures varied from 14.7 to 20.6 °C (Table 2). Total alkalinity and DIC concentrations (average TA = 2.60 ± 0.01 mM and

average DIC = 2.30 ± 0.02 mM, Table 2) were relatively high compared to the Mediterranean Sea average, but common for the Gulf of Lions (Cossarini et al., 2015). The pH_T of the bottom waters varied from 8.05 to 8.09 with the highest value observed at station AK and the lowest at station E. Although the oxygen concentration decreased with water depth, bottom waters were always well ventilated, with dissolved O_2 concentrations higher than 220 µmol L^{-1}. Sediment porosity ranged between 0.7 and 0.8 at the SWI, and they were similar at all stations between 20 and 400 mm depth (Table 2).

3.2 Benthic total and diffusive fluxes

The *in situ* pH and O_2 microprofiles reflected the differences between the three study domains under the influence of the Rhône River plume (Fig. 2). In the proximal zone (stations A and Z), the oxygen penetration depth was only 1.5 to 2.5 mm into the sediment as also indicated by separate voltammetric measurements (Fig. 5). The oxygen penetration depth increased from 2 to 6 mm at station K and reached 8 to 11 mm at the most offshore station E. As a result of bad weather conditions, no exploitable *in situ* microprofiles were recorded at stations AK and B, though *ex situ* voltammetric profiles determined oxygen penetration depths of 4 and 2 mm, respectively (Fig. 5). All pH microfiles indicated a pH minimum between 7.2 and 7.4 just below the OPD followed by an increase to between 7.5 and 7.6 in the manganous/ferruginous layers of the sediment around 5 mm inshore and below 12 mm offshore (Fig. 2). Below this depth, pH stabilizes.

The benthic chamber was deployed once at stations A and E and twice at station Z (Z' is the replicate). Total alkalinity and DIC concentrations increased linearly with time in the chamber, but concentration changes decreased along the nearshore-offshore transect (Fig. 3). The highest benthic fluxes were recorded for the two deployments at station Z, with TA fluxes of 73.9 ± 20.6 and 56.0 ± 17.8 mmol m^{-2} d^{-1} and DIC fluxes of 78.3 ± 10.9 and 37.2 ± 7.2 mmol m^{-2} d^{-1} (Fig. 4, Table 2). At station A, the benthic TA and DIC fluxes reached lower values of 14.3 ± 1.6 and 17.8 ± 1.6 mmol m^{-2} d^{-1}, respectively, while benthic fluxes were lowest at station E, with a TA flux of 3.7 ± 0.9 mmol m^{-}

^{2} d^{-1} and a DIC flux of 9.9 ± 0.9 mmol m^{-2} d^{-1}. In parallel, DOU fluxes reached 10.2 ± 1.3 and 10.4 ± 0.9 mmol m^{-2} d^{-1} at stations A and Z and decreased offshore to 5.9 ± 1.0 mmol m^{-2} d^{-1} at station K and 3.6 ± 0.6 mmol m^{-2} d^{-1} at station E (Fig. 4, Table 2). Although the relative importance of DOU compared to TA and DIC fluxes increased offshore, the TA and DIC fluxes were always between 2 and 8 times larger than the DOU fluxes (Fig. 4).

3.3 Electrochemistry profiles

Dissolved Fe^{2+} concentrations as a function of depth in the sediment mirrored the voltammetric signals of soluble organic-Fe(III) complexes at stations A, Z, AK, B, and K (Fig. 5). High concentrations of dissolved Fe^{2+} were observed in the proximal domain at stations A (341 ± 22 µM) and Z (234 ± 25 µM), where dissolved ΣH_2S was not detected (Fig. 5). At station AK, the shallowest station in the prodelta domain, dissolved Fe^{2+} increased to a maximum concentration of 255 µM around 2 cm depth, then decreased with sediment depth as FeS_{aq} below 6.5 cm and small concentrations of dissolved ΣH_2S around 17 cm were produced (Fig. 5). The two deeper prodelta stations, B and K, displayed lower Fe^{2+} concentrations, including one peak not exceeding 81 µM (station B) or 73 µM (station K) in the top 2 cm of the sediment and a second peak not exceeding 50 µM between 12-14 cm (station B) and 86 µM between 5-7.5 cm (station K) in the sediment. Although FeS_{aq} was only detected below 15 cm at station K, ΣH_2S was produced in low concentrations (< 5 µM) around 6.5 cm at stations B and K (Fig. 5). A peak of Fe^{2+} was initially formed in the top 5 cm of the distal domain (station E) but decreased to a minimum value with depth and did not correlate with the organic-Fe(III) voltammetric signals, which also remained low throughout the profile (Fig. 5). Finally, station E displayed generally low concentrations of ΣH_2S in the pore waters (< 6 µM), though the onset of ΣH_2S production was much shallower (2.5 cm) and ΣH_2S concentrations were consistently higher throughout the profile than at any other stations.

Biogeosciences Discuss., https://doi.org/10.5194/bg-2019-32
Manuscript under review for journal Biogeosciences
Discussion started: 4 February 2019

3.4 Geochemical characteristics of the pore waters and sediments

Both TA and DIC concentrations increased rapidly within the pore waters (Fig. 6), likely reflecting the intensity of organic carbon mineralization rates in these sediments. At all stations, DIC pore water concentrations correlated well with TA (overall slope: 1.01 ± 0.006, r^2=0.995, n=134). The TA and DIC gradients were highest at stations A and Z, where maximum concentrations of both species reached around 55 mM. At station AK, TA and DIC concentrations reached a maximum of 15 mM at 25 cm depth but decreased to 6 mM at the bottom of the core. The maximum concentrations of TA and DIC of 35 mM observed at station B, were more comparable to the stations in the vicinity of the river mouth (stations A and Z) than other stations located in the prodelta domain (stations AK and K). At station K, TA and DIC concentrations reached 10 mM, whereas the lowest TA and DIC gradients were measured at station E, with concentrations reaching only 4.6 mM at the bottom of the cores (30 cm). Sulfate was completely removed from the pore waters at depths of 35, 24, and 45 cm at station A, Z, and B, respectively (Fig. 6). In turn, sulfate concentrations decreased to a minimum concentration of 20 mM at 29 and 24 cm depth at stations AK and K, whereas sulfate consumption was much smaller at station E with a minimum concentration of 28 mM (bottom water sulfate concentration was 31.4 mM). As a result, TA and DIC changes in concentration at a given depth were highly inversely correlated ($r^2 > 0.97$) with sulfate changes in concentration at stations A, Z, AK, B, and K (Table 3). At station E, sulfate variations in the observed depth were in the same order of magnitude as the measuring uncertainties. Simultaneously, TA and DIC demonstrated strong correlations ($r^2 > 0.97$) at stations A, Z, AK, B, and K (Table 3). In the proximal domain (stations A and Z), ammonium increased with sediment depth to concentrations > 3 mM (Fig. 6). At station B, ammonium reached concentrations > 2 mM with depth, whereas ammonium concentrations did not exceed 1.5 mM at station AK, 0.6 mM at station K, and 0.3 mM at station E. At all stations nitrite plus nitrate concentrations were less than 20 µM (data not shown). Significant methane concentrations (> 50 µM) were detected at the bottom of the sediment core at stations A, Z, and AK (Fig. 6), and a SMTZ was identified between 28 and 39 cm at station A and between 19 and 39 cm at

station Z. As methane was < 50 µM throughout the profile at station K and sulfate was not completely consumed inside the sediment core at station AK, the SMTZ was not determined at these two stations. Methane analyses were not carried out for the other stations.

The sediment pore waters were oversaturated with respect to calcite ($\Omega_{Ca} > 1$) at all stations. At stations A, Z, and B, decreasing Ca^{2+} concentrations in the pore waters indicated precipitation of $CaCO_3$, whereas Ca^{2+} concentrations remained close to the bottom water Ca^{2+} concentrations (11.2 mM in Mediterranean waters) at the other stations (Fig. 6). Dissolved phosphate concentrations (ΣPO_4^{3-}) were relatively high (50-100 µM) throughout the profiles at stations A, AK, K and Z, and a large increase in concentration (up to 160 µM at station Z) was observed at station AK, K and Z between 15 and 22 cm. In turn, ΣPO_4^{3-} production was minimal throughout station E pore waters (< 10 µM). Dissolved phosphate was not measured at station B. Sediment samples were analyzed for AVS as a function of depth at stations A, AK, and E to assess one station in each domain (Fig. 6). At station A, a peak in AVS (65 µmol g^{-1}) was measured around 8.0 cm followed by a second, smaller peak (22 µmol g^{-1}) at 14 cm, after which AVS decreased with depth. The AVS concentrations were low in the top portion of the sediment at station AK but increased with depth to 100 µmol g^{-1} around 15 cm. At station E, only a small AVS peak of 20 µmol g^{-1} was observed at 14 cm. Finally, large concentrations of FeS nanoparticles (FeS_0) were found in the proximal and prodelta stations, including two broad peaks and maximum concentrations around 1 mM at stations A and Z and a large subsurface maximum up to 6 mM at 145 mm at station AK. These FeS_0 concentrations increased as a function of depth to a relatively constant 0.5 mM below 4.5 cm at station B and below 12 cm at station K, whereas they remained mostly negligible at station E (Fig. 6).

4. Discussion

In this study, we want to relate biogeochemical processes in the sediment to the observed TA and DIC fluxes. Firstly, benthic TA and DIC fluxes in the Rhône River prodelta are compared to other similar systems to evaluate their relative importance. In the following sections, the most likely

biogeochemical processes responsible for the high TA flux are identified based on the sediment depth profiles collected. In particular, the role of iron sulfide mineral precipitation on the benthic TA flux is established using a variety of analytical techniques, speciation calculations, and a mass balance approach. Finally, the link between inputs to the sediment, carbon mineralization processes, sulfide mineral burial, and the benthic TA flux is provided using a conceptual model.

4.1 DIC and alkalinity fluxes from the sediment

The sediments of the Rhône proximal and prodelta zones represent important sources of both DIC and TA to the bottom waters (Fig. 4). The DIC fluxes observed in the proximal domain (18-78 mmol m^{-2} d^{-1} at station A and Z; Fig. 4) are in the range of previously measured fluxes in other deltas where anaerobic mineralization processes are dominant, including Mississippi delta sediments from core incubations (15-20 mmol m^{-2} d^{-1}; Lehrter et al., 2012) or benthic chambers (36-53 mmol m^{-2} d^{-1}; Rowe et al., 2002), benthic chamber measurements of the Po River delta sediments and the Adriatic shelf (15-25 mmol m^{-2} d^{-1} ; Hammond et al., 1999), or the Fly River delta during the most active season (35-42 mmol m^{-2} d^{-1} ; Aller et al., 2008) and near the Guadalquivir River estuary (36-46 mmol m^{-2} d^{-1}, Ferron et al., 2009). In contrast, fewer alkalinity fluxes were measured in river deltas, though those obtained from benthic chambers in the Danube and Dniester deltas in the Northwest Black Sea (21-67 mmol m^{-2} d^{-1}, Friedl et al., 1998), are within the range of values reported in this study (14-74 mmol m^{-2} d^{-1}). Benthic TA fluxes obtained in the Guadalquivir estuary (24-30 mmol m^{-2} d^{-1}; Ferron et al., 2009) and the Adriatic shelf sediments off the Po River delta (0.5-10.4 mmol m^{-2} d^{-1}; Hammond et al., 1999) are in the lower range of TA fluxes measured in the present study. The biogeochemical origin of these TA benthic fluxes is discussed in the next sections.

4.2 The relative importance of nitrification/denitrification on the TA budget

Denitrification is known as a benthic TA source to the bottom waters as 0.8 moles of TA are produced for 1 mole of organic carbon oxidized by nitrate and the product N_2 does not react further

with dissolved oxygen (Table 1, Eq. 5; Thomas et al., 2009; Krummins et al., 2013; Brenner et al., 2016). Published estimates of total denitrification rates in Rhône prodelta and shelf sediments range between 4 mmol m^{-2} d^{-1} in the proximal zone to 1 mmol m^{-2} d^{-1} in the continental shelf (Pastor et al., 2011). Conversion to alkalinity flux would provide a range between 0.8 and 3.2 mmol TA m^{-2} d^{-1}. As such, denitrification would account for < 10% of the TA flux in the proximal zone where substantial fluxes were measured by *in situ* benthic chambers (Fig. 4). Furthermore, the only net production of TA by denitrification must be related to external nitrate sources as nitrification (overall oxidation of ammonium to nitrate) consumes 2 moles of TA per mole of ammonium transformed into nitrate (Table 1, Eq. 2; Hu et al., 2011a). As coastal sediments mostly display coupled nitrification-denitrification, this process does only represent a small source of TA to the bottom waters (Brenner et al., 2016). It can therefore be concluded that the contribution of denitrification to TA fluxes is minimal in the proximal zone and could be proportionally more important on the shelf where TA fluxes are much lower.

4.3 DIC and TA produced by sulfate reduction

Sulfate reduction typically represents a major organic carbon mineralization pathway in organic-rich sediments that simultaneously produces two moles of total alkalinity (TA) and two moles of DIC per mole of sulfate (Table 1, Eq. 6) (Canfield et al., 1993b; Burdige, 2011). Dissimilatory iron reduction (Table 1, Eq. 7) in turn produces 1/4 moles of DIC and consumes 7/4 moles of H^+, resulting in two moles of TA produced per mole of Fe. As these two processes equally produce two moles of TA per mole of terminal electron acceptor (Table 1, Eq.6 for SO_4^{2-} and Eq. 7 for $Fe(OH)_3$), they can both contribute significantly to the bulk alkalinity production in sediment pore waters. The low concentration of nitrate, relatively low production of reduced metals in the pore waters (Fig. 5), and intense ammonium and DIC production in parallel with sulfate consumption at depth (Fig. 6) confirm that sulfate reduction is one of the dominant mineralization pathways in the Rhône prodelta sediments (Pastor et al., 2011; Rassmann et al., 2016). Experimentally-derived stoichiometric ratios of the

relative production of DIC and TA compared to sulfate consumption may indicate the dominant reaction pathways responsible for the high alkalinity generated in these sediments (Burdige and Komada, 2011). Factoring carbonate precipitation using the pore water Ca^{2+} data, the r_{DSc} were determined to range between -2.05 and -1.86, except for one value at -1.37 (station B), whereas the r_{ASc} ratios ranged between -2.35 and -1.89 with the exception of station B at -1.58 (Table 3). Theoretically, the r_{DS} and r_{AS} should equal -2.0 if sulfate reduction is the only control on DIC and TA production (Table 1, Eq. 6), suggesting that, except at station B, the influence of other diagenetic processes on r_{ASc} and r_{DSc} is limited. At station B, however the higher r_{DSc} ratio (Table 3) may indicate significant anaerobic oxidation of methane (AOM Table 1, Eq. 8) which generates a theoretical r_{DS} of -1 (Borowsi et al., 1996; Komada et al., 2016). Unfortunately, methane sampling was not performed at station B, preventing precise identification of AOM at this station.

4.4 Formation of iron sulfide species

Although the complete depletion of sulfate in the first 30 cm of the sediment at stations A, Z, and B implies an equivalent production of dissolved sulfide (ΣH_2S) (Table 1, Eq. 6), pore waters displayed little to no ΣH_2S (Fig. 5). If all of the produced ΣH_2S diffused upward and reacted in the oxic sediment layer, the alkalinity produced by sulfate reduction would be consumed by the oxidation of ΣH_2S by dissolved O_2 and the pH should be lowered significantly given the large acidity generated by this reaction (Table 1, Eq. 4). Although ΣH_2S was nearly absent of the pore waters (Fig. 5), the pH minimum was never lower than 7.2 and the observed alkalinity fluxes across the SWI were substantial (Fig. 4), indicating that ΣH_2S was removed from the pore waters below the oxic layer. Abiotic reduction of Fe(III) oxides by ΣH_2S (Table 1, Eq. 9), followed by precipitation of FeS in the anoxic zone (Table 1, Eq. 10; Berner, 1970; Pyzik and Sommer, 1981; Carman and Rahm, 1997, Soetaert et al., 2007), and eventually formation of pyrite (Table 1, Eq. 11; Rickard and Luther, 1997) may represent a significant ΣH_2S removal pathway. As the abiotic reduction of Fe(III) oxides by ΣH_2S coupled with either FeS or FeS and pyrite precipitation (Table 1, Eq. 9-11) does overall not alter

Biogeosciences Discuss., https://doi.org/10.5194/bg-2019-32
Manuscript under review for journal Biogeosciences
Discussion started: 4 February 2019

alkalinity, bacterial sulfate reduction followed by abiotic precipitation of iron and sulfide from the pore waters to either FeS or pyrite (Table 1, Eqs. 12 and 13) should result in r_{AD} = 1 and r_{DS} = r_{AS} = -2. Formation of pyrite is accompanied by the consumption of molecular H_2 by sulfate-reducing bacteria, resulting in a slight increase in the r_{AD} and r_{DS} to 1.1 and -1.81 for the overall reaction while the r_{AS} ratio should not change (Table 1, Eq. 14). Another possible pathway includes the concomitant production of Fe^{2+} by dissimilatory iron reduction (Table 1, Eq. 7) and ΣH_2S by sulfate reduction followed by precipitation of FeS. In this case, the net r_{AD} and r_{DS} ratios should decrease to 0.89 and -2.25, whereas the r_{AS} ratio should remain at -2 (Table 1, Eq. 15). With ensuing formation of pyrite, theoretical mole ratios may change slightly to r_{AD} = 0.94 and r_{DS} = -2.13 without H_2 reoxidation (Table 1, Eq. 16), whereas r_{AD} and r_{DS} ratios of 1.06 and -1.89 should be reached with H_2 reoxidation by sulfate-reducing bacteria (Table 1, Eq. 17). In both cases, the r_{AS} ratio should remain at -2.

The observed range of r_{ADc} (1.06 to 1.15) and r_{DSc} (-2.05 to -1.86) ratios in the proximal and prodelta stations, except at station B (Table 3), is fully compatible with sulfate reduction coupled to iron reduction and FeS precipitation (possibly followed by pyritization), though r_{ADc} and r_{DSc} ratios are not able to distinguish abiotic and microbial pathways of iron reduction. The occurrence of dissimilatory iron reduction in the proximal and prodelta domains, however, is substantiated by several other pieces of evidence. First, the production of soluble organic-Fe(III) complexes deeper than the oxygen penetration depths (Fig. 5) indicates that these species did not result from the oxidation of Fe^{2+} by dissolved O_2 in the presence of organic ligands (Taillefert et al., 2000). Second, as soluble organic-Fe(III) complexes are produced as intermediates in the reduction of Fe(III) oxides by iron reducing bacteria (Taillefert et al., 2007; Jones et al., 2010), their concomitant detection with Fe^{2+} at all the stations in the proximal and prodelta domains (Fig. 5) suggests they were produced during dissimilatory iron reduction. Third, the positive correlation between the current intensities of organic-Fe(III) complexes and Fe^{2+} concentrations is in line with the same correlation obtained in iron-rich deep-sea sediments (Fig. 7) where sulfate reduction was not significant (Beckler et al., 2016). Finally, as these organic-Fe(III) complexes are readily reduced by ΣH_2S (Taillefert et al.,

2000), their presence in zones of sulfate reduction suggest these sediments are highly dynamic with periods of intense sulfate reduction alternating with periods during which sulfate reduction is repressed and replaced by microbial iron reduction. These dynamics may be controlled by the input of organic and inorganic material from the Rhône River in the proximal domain, especially during floods when most of the solid material is deposited on the seafloor (Cathalot et al., 2010; Pastor et al., 2018).

4.5 FeS precipitation

The discrepancy between sulfate consumption and the low concentration of ΣH_2S along with the high TA fluxes clearly suggest that much of the sulfur was precipitated in the solid phase. Indeed, AVS measurements show precipitation of FeS in the proximal and prodelta domains (Fig. 6). In addition, the large phosphate concentrations observed at depth in the proximal and prodelta domains (Fig. 6) suggest that ΣPO_4^{3-} adsorbed to Fe(III) oxides was released in the pore waters during secondary conversion of Fe(III) oxides to FeS (Anschutz et al., 1998; Rozan et al., 2002). More importantly, large concentrations of nanoparticulate FeS (FeS_0 in the range of 1-6 mM) were identified in the proximal and prodelta stations that decreased with distance from shore (Fig. 6). The existence of FeS_0 suggests that large fractions of Fe^{2+} and ΣH_2S were actively removed from the pore waters at the time of measurements and eventually immobilized under the form of sulfide minerals. Although soluble FeS_{aq} clusters detected electrochemically when the system is oversaturated with respect to FeS (Theberge and Luther, 1997) are considered good indicators of the active precipitation of iron sulfide minerals (Luther and Ferdelman, 1993; Davison et al., 1998; Taillefert et al., 2000), they were rarely observed in the Rhône River delta (Fig. 5). Indeed, the ion activity products (pIAPs) calculated at most stations indicate that pore waters were either undersaturated, as a result of the low concentrations (stations AK, B, and K) or complete absence (stations A and Z) of dissolved sulfides, or close to the solubility of amorphous FeS or mackinewite (Fig. 8). Collectively, the large concentrations of dissolved FeS_0 compared to the small electrochemically active FeS_{aq} complexes

and the generally low saturation state of the pore waters indicate that FeS was much more aggregated during this time period. Overall, the presence of soluble organic-Fe(III) complexes along with dissolved Fe^{2+} throughout the profiles, the absence of ΣH_2S and FeS_{aq}, and the large concentrations of dissolved FeS_0 found in the pore waters despite complete removal of sulfate in the proximal and some of the prodelta stations provide strong evidence of large FeS precipitation in a context where sulfate-reducing conditions may alternate with iron-reducing conditions as already observed seasonally in estuarine sediments (Taillefert et al., 2002).

4.6. Benthic alkalinity flux as a result of iron sulfide burial

As the extreme sedimentation rates (> 30 cm yr^{-1}) in the proximal domain prevent short-term reoxidation of ΣH_2S, the burial of FeS should represent a net source of alkalinity in the pore waters (Berner, 1982; Hu and Cai, 2011a; Brenner et al., 2016). With the precipitation of FeS, about 2 to 3 moles of alkalinity equivalent should be produced for each mole of sulfur precipitated (Table 1, Eqs. 12 and 15). Assuming concomitant dissimilatory iron and sulfate reduction dominate in the proximal and prodelta zones, a conservative ratio of 2 moles of TA equivalent per mole of FeS precipitated can be estimated (Table 1, Eq. 15). In this calculation, the alkalinity production flux was estimated from the average AVS burial fluxes using Eq. 5, with the caveat that these flux comparisons are made assuming steady-state which is questionable in such a dynamic system. Nonetheless, the average AVS concentration of the proximal station (station A) was used, as the sedimentation rate at this station is so high (>30 cm y^{-1}) that the entire sediment layer investigated is buried rapidly in a year. The calculated AVS burial flux provides an alkalinity-equivalent flux of 25.0 ± 7.7 mmol m^{-2} d^{-1} in the proximal domain (Table 4), which falls within the range of benthic alkalinity fluxes measured by benthic chamber at stations A and Z (14.3 - 73.9 mmol m^{-2} d^{-1}; Fig. 4 and Table 4). In the prodelta, the alkalinity-equivalent flux is estimated at 9.8 ± 2.8 mmol m^{-2} d^{-1} at station AK (Table 4), which unfortunately cannot be compared to benthic alkalinity fluxes as they were not measured. In the distal domain, however, a low alkalinity-equivalent flux of 0.04 ± 0.1 mmol m^{-2} d^{-1} is estimated from the

average AVS burial flux at station E. This flux is much lower than the 3.7 ± 0.9 mmol m^{-2} d^{-1} flux measured by benthic chamber (Fig. 4), a difference that could be due to denitrification and shallow carbonate dissolution.

4.7. Benthic alkalinity flux as a result of carbonate dissolution

Calcium carbonate dissolution below the sediment-water interface as a result of the acidity generated by aerobic respiration may represent another possible contributor to TA fluxes as demonstrated in carbonate-rich permeable sediments (Burdige and Zimmerman, 2002; Cyronak et al., 2013; Rao et al., 2014). Both the water column (Ω_{Ca} = 5.5) and the pore waters (Ω_{Ca} > 1) of the proximal zone are largely oversaturated with respect to calcite (Rassmann et al., 2016; Fig. 6). These findings are corroborated by a large decrease in Ca^{2+} concentration in the pore waters, indicating $CaCO_3$ precipitation at depth in proximal zone sediments. Yet, the intense consumption of dissolved oxygen in the first millimeters below the sediment-water interface generates a large pH decrease (Fig. 2) that may induce carbonate dissolution at this scale. Calcium carbonate saturation states at a millimeter scale near the SWI were calculated from pH profiles and an interpolation of the centimetre-scale DIC profiles using the SeaCarb software (Fig. 9). They show that in the proximal zone, the saturation state with respect to calcite, which is the most abundant detrital carbonate in these sediments (Rassmann et al., 2016), is always above 1.5. Such saturation state precludes massive carbonate dissolution at the sediment surface and discounts shallow carbonate dissolution as playing a large role on the benthic alkalinity fluxes observed in the proximal sediments. Minor quantities of calcium carbonate may be dissolved in microniches where the pH could be lower than 7.4 or less abundant carbonate forms (aragonite) may dissolve in the millimetric layers where this mineral is close to undersaturation. These processes, however, surely represent an insignificant flux in the proximal zone compared to the large alkalinity generated by sulfate reduction and subsequent FeS burial. At the distal station on the shelf (Station E, Fig. 9c), the saturation state was close to 1 which may indicate a potential contribution of calcium carbonate dissolution to the benthic alkalinity flux.

Biogeosciences Discuss., https://doi.org/10.5194/bg-2019-32
Manuscript under review for journal Biogeosciences
Discussion started: 4 February 2019

4.8. Linking TA and DIC fluxes to mineralization processes

Overall, the present findings indicate that FeS burial modifies the alkalinity budget in the proximal and prodelta sediments (Brenner et al., 2016). As the order of magnitude of the measured benthic alkalinity fluxes is compatible with the alkalinity generated during the reduction of Fe(III) oxides, sulfate, and subsequent FeS burial in the proximal zone, these processes are likely responsible for the large alkalinity fluxes reported in this high-sedimentation delta and, potentially, other similar systems (Hu and Cai, 2011a).

The biogeochemical cycling of C, Fe, S, and TA close to the Rhône River mouth can be theoretically summarized as follows (Fig. 10): (i) the high pore water DIC concentrations resulting from the production of metabolic CO_2 during organic carbon mineralization lead to benthic DIC fluxes that are only modulated by the precipitation of carbonate minerals; (ii) the high pore water TA concentrations result from intense iron and sulfate reduction as a result of the high supply of organic matter and Fe(III) oxides to the sediment; (iii) the precipitation of FeS and the high sedimentation rates near the river mouth preserve the majority of reduced iron and ΣH_2S buried in the form of FeS minerals and potentially pyrite within the anoxic sediments (Aller et al., 1986); and (iv) ultimately, the TA-consuming reoxidation of reduced metabolites (i.e., NH_4^+, ΣH_2S, Fe^{2+}) is not important in the oxic sediment layers, and a significant fraction of the anaerobically-produced TA is transferred across the SWI (Fig. 10, red dashed line). In these conditions, anaerobic and aerobic processes are decoupled, and the consumption of oxygen no longer reflects the overall respiration rates within these sediments (Pastor et al., 2011) as observed by the relatively lower contribution of DOU fluxes compared to TA and DIC fluxes in the proximal domain (Fig. 4).

In contrast, sedimentation rates (Table 2), overall respiration rates (Fig. 4), and the intensity of iron and sulfate reduction (Fig. 6) decrease in the distal domain (station E), and as a consequence the relative proportion of aerobic processes increases (Pastor et al., 2011). Despite the relatively small decrease in pore water sulfate concentrations with depth and low ΣH_2S concentrations (< 10 µmol L^{-1}) at the most offshore station E, ΣH_2S concentrations were the highest of all the stations. These

findings likely reflect the fact that less riverine Fe(III) oxides were available for FeS precipitation. With low sedimentation rates (0.1 to 1 cm yr^{-1}) and thus low input of organic matter and Fe(III) oxides, the overall carbon turnover is decreased and the reduced by-products of sulfate and/or iron reduction may be transported back to the oxic sediment layers to be reoxidized by dissolved oxygen. In this case, the alkalinity generated by anaerobic respiration processes is consumed by reoxidation of the reduced metabolites, and the flux of alkalinity near the SWI decreases to weak values at station E (Fig. 4 and Fig. 10, black line).

The strong TA flux to the overlying waters measured in the Rhône River delta, may contribute, along with riverine inputs, to the overall high alkalinity of the Gulf of Lions waters compared to the Mediterranean average (Cossarini et al., 2015). However, the influence of the benthic TA flux on the water column pH and ultimately on the absorption of atmospheric CO_2 depends mainly on the TA to DIC benthic flux ratio (F_{TA}/F_{DIC}), vertical mixing in the water column, and thus the residence time of the bottom waters (Hu and Cai, 2011b, Andersson and Mackenzie, 2012). The F_{TA}/F_{DIC} ratios, ranging between 0.8 and 1 in the proximal and prodelta zones of the Rhône River delta (Fig. 11), are in the high range of a compilation of TA to DIC flux ratios obtained in different coastal systems and continental shelves (expanded from Hu and Cai, 2011b). As these ratios do not exceed 1, alkalinity generated in the sediments will not decrease pCO_2 in the bottom waters and thus not draw atmospheric CO_2 into the coastal ocean. Yet, the large benthic TA fluxes generated from deltaic sediments and the elevated F_{TA}/F_{DIC} (>0.8), which were unknown in the Rhône River prodelta before this study, may modify the carbonate cycle paradigm in these coastal regions.

5. Conclusion

In this study, benthic respiration, as well as benthic alkalinity and DIC fluxes were quantified in the Rhône River delta using benthic landers. These measurements demonstrated that sediments from the proximal and prodelta domains represent a strong source of alkalinity to the water column. The highest alkalinity and DIC fluxes were detected in the vicinity of the Rhône River mouth and were

much stronger than fluxes of dissolved oxygen, indicating the decoupling of oxic and anoxic biogeochemical processes. As pore water oversaturation with respect to calcite prevented carbonate dissolution to occur over the entire sediment column, the high benthic alkalinity fluxes resulted from the high intensity of anaerobic respiration processes, mainly via sulfate reduction and precipitation of iron sulfide minerals, but also with some contributions from dissimilatory iron reduction and AOM. The intensity of sulfate reduction in the proximal domain also resulted in the consumption of a 10-20% fraction of the alkalinity and DIC by the precipitation of authigenic carbonates. As the reduced metabolites Fe^{2+} and $\sum H_2S$ produced by the mineralization of organic matter were buried in the solid phase, alkalinity was not consumed by their reoxidation in the oxic sediment layers. Consequently, a significant fraction of the total alkalinity generated in the pore waters was transferred to the bottom waters (benthic flux of 14-74 mmol m^{-2} d^{-1}). Although sulfate reduction dominated the proximal and prodelta domains, evidence for dissimilatory reduction of Fe(III) oxides was simultaneously observed in the depth profiles, suggesting that anaerobic processes in the Rhône River prodelta are dynamic and potentially controlled by pulsed sediment accumulations. The intensity of the alkalinity and DIC fluxes decreased offshore as the sedimentation rate and the relative importance of anaerobic mineralization pathways compared to aerobic processes decreased. In these conditions the more "classical" coupling between aerobic and anaerobic reactions occurs, hence producing much lower benthic alkalinity fluxes. Overall, these findings suggest that deltaic sediments exposed to large riverine inputs of inorganic and organic material may provide a large source of alkalinity to the overlying waters and thus weaken the increase in pCO_2 more significantly than previously thought in coastal waters.

Acknowledgments

The authors thank the captain and crews of the RV Tethys II for their support at sea and Bruno Bombled for his technical help on-board and in the laboratory. We thank Gael Monvoisin for the analysis of sulfate samples at GEOPS (Paris-Sud University), Joel Craig and Olivia Studebaker for

the analysis of nutrients and AVS at Georgia Tech, and Celine Liorzou for the ICP-AES measurements at Pôle Spéctrométrie Océan in Brest. We are grateful to Sabine Kasten, Sandra Arndt, and Andrew Dale for interesting discussions about the interactions of AOM with carbonates and iron minerals and sediment dynamics. This research was funded by the project Mistrals/MERMEX-Rivers and AMORAD (ANR-11-RSNR-0002) and the National Science Foundation (OCE-1438648).

References

Aller, R. C., Blair, N. E., and Brunskill, G. J.: Early diagenetic cycling, incineration, and burial of sedimentary organic carbon in the central Gulf of Papua (Papua New Guinea). J. Geophys. Res., 113: 1–22, 2008.

Aller, R. C., Mackin, J. E., and Cox, R. T.: Diagenesis of Fe and S in Amazon inner shelf muds: apparent dominance of Fe reduction and implications for the genesis of ironstones. Cont. Shelf. Res., 6: 263–289, 1986.

Andersson, A.J., Mackenzie, F.T. and Lerman, A: Coastal ocean CO_2-carbonic acid-carbonate sediment system of the anthropocene. Glob. Biogochem. Cycle, 20, GB1S92, 2006.

Andersson, A. and Mackenzie, F.: Revisiting four scientific debates in ocean acidification research. Biogeosci., 9: 893–905, 2012.

Anschutz, P., Zhong, S., Sundby, B., Mucci, A., and Gobeil, C.: Burial efficiency of phosphorus and the geochemistry of iron in continental margin sediments. Limnol. Oceanogr., 43: 53–64, 1998.

Bauer, J. E., Cai, W.-J., Raymond, P. A., Bianchi, T. S., Hopkinson, C. S., and Regnier, P. A. G.: The changing carbon cycle of the coastal ocean. Nature, 504(7478): 61–70, 2013.

Beckler, J., Nuzzio, D., and Taillefert, M.: Development of single-step liquid chromatography methods with ultraviolet detection for the measurement of inorganic anions in marine waters. Limnol. Oceanogr. Meth., 12: 563–576, 2014.

Beckler, J. S., Kiriazis, N., Rabouille, C., Stewart, F. J., and Taillefert, M.: Importance of microbial iron reduction in deep sediments of river-dominated continental-margins. Mar. Chem., 178: 22–34, 2016.

Ben-Yaakov, S.: pH buffering of pore water of recent anoxic marine sediments. Limnol. Oceanogr., 18(1): 86–94, 1973.

Berelson, W.M. et al.: Biogenic matter diagenesis on the sea floor: A comparison between two continental margin transects. J. Mar. Res., 54: 731-762, 1996.

Berner, R. A.: Sedimentary pyrite formation. Am. J. Sci., 268: 1–23, 1970.

Berner, R. A.: Early Diagenesis: A Theoretical Approach. Princeton University Press, 1980.

Berner, R. A.: Burial of organic carbon and pyrite sulfur in the modern ocean; its geochemical and environmental significance. Am. J. Sci., 282: 451–473, 1982.

Bianchi, S. T. and Allison, M. A.: Large-river delta-front estuaries as natural ‘‘recorders’’ of global environmental change. Proc. Natl. Acad. Sci. U.S.A., 106: 8085–8092, 2009.

Borowski, W. S., Pau, C. K., and Ussler, W.: Marine pore-water sulfate profiles indicate in situ methane flux from underlying gas hydrate. Geol., 24(7): 655–658, 1996.

Brenner, H., Braeckman, U., Le Guitton, M., and Meysman, F. J. R.: The impact of sedimentary alkalinity release on the water column CO_2 system in the North Sea. Biogeosci., 13: 841–863, 2016.

Bristow, G. and Taillefert, M.: VOLTINT: A Matlab (R)-based program for semi-automated processing of geochemical data acquired by voltammetry. Comp. Geosci., 29: 153–162, 2008.

Broecker, W. S. and Peng, T.-H.: Gas exchange rates between air and sea. Tellus, 26: 21–35, 1974.

Buffle, J.: Complexation reactions in aqueous systems: An Analytical Approach. Wiley and Sons, 1988.

Bura-Nakic, E., Viollier, E., Jezequel, D., Thiam, A., and Ciglenecki, I.: Reduced sulfur and iron species in anoxic water column of meromictic crater Lake Pavin (Massif Central, France). Chem. Geol., 266:311–317, 2009.

Burdige, D.J., Zimmerman, R.C.: Impact of sea grass density on carbonate dissolution in Bahamian sediments. Limnol. Oceanogr., 47, 1751-1763, 2002.

Burdige, D.: Burial of terrestrial organic matter in marine sediments: A re-assessment. Glob. Biogeochem. Cycles. 19. GB4011, doi:10.1029/2004/GB002368, 2005.

Burdige, D.: Estuarine and Coastal Sediments - Coupled Biogeochemical Cycling. Treat. Estuar. Coast. Sci., 5: 279–316, 2011.

Burdige, D. J. and Komada, T.: Anaerobic oxidation of methane and the stoichiometry of remineralization processes in continental margin sediments. Limnol. Oceanogr., 56(5): 1781–1796, 2011.

Cai, W.-J.: Estuarine and Coastal Ocean Carbon Paradox: CO_2 Sinks or Sites of Terrestrial Carbon Incineration? Ann. Rev. Mar. Sci., 3(1): 123–145, 2011.

Cai, W.-J. and Reimers, C. E.: The development of pH and pCO_2 microelectrodes for studying the carbonate chemistry of pore waters near the sediment-water interface. Limnol. Oceanogr., 38:1762–1773, 1993.

Canfield, D. E., Jørgensen, B. B., Fossing, H., Glud, R., Gundersen, J., Ramsing, N. B., Thamdrup, B., Hansen, J. W., Nielsen, L. P., and Hall, P.O.J.: Pathways of organic carbon oxidation in three continental margin sediments. Mar. Geol., 113: 27–40, 1993a.

Canfield, D. E., Thamdrup, B., and Hansen, J. W.: The anaerobic degradation of organic matter in Danish coastal sediments: iron reduction, manganese reduction, and sulfate reduction. Geochim. Cosmochim. Acta, 57(16): 3867–3883, 1993b.

Carman, R. and Rahm, L.: Early diagenesis and chemical characteristics of interstitial water and sediments in the deep deposition bottoms of the Baltic proper. J. Sci. Res., 37: 25–47, 1997.

Cathalot, C., Rabouille, C., Pastor, L., Deflandre, B., Viollier, E., Buscail, R., Grémare, A., Treignier, C., and Pruski, A.: Temporal variability of carbon recycling in coastal sediments influenced by rivers: assessing the impact of flood inputs in the Rhône River prodelta. Biogeosci., 7:1187–1205, 2010.

Cathalot, C., Rabouille, C., Tisnérat-Laborde, N., Toussaint, F., Kerhervé, P., Buscail, R., Loftis, K., Sun, M.-Y., Tronczynski, J., Azoury, S., Lansard, B., Treignier, C., Pastor, L., and Tesi, T.: The fate of river organic carbon in coastal areas: A study in the Rhône River delta using multiple isotopic ($\delta^{13}C$, $\Delta^{14}C$) and organic tracers. Geochim. Cosmichim. Acta, 118:33–55, 2013.

Charmasson, S., Radakovitch, O., Arnaud, M., Bouisset, P., and Pruchon, A.-S.: Long-core profiles of ^{137}Cs, ^{134}Cs, ^{60}Co and ^{210}Pb in sediment near the Rhône River (Northwestern Mediterranean Sea). Estuaries, 21(3):367–378, 1998.

Chen, C.-T. A. and Borges, A. V.: Reconciling opposing views on carbon cycling in the coastal ocean: Continental shelves as sinks and near-shore ecosystems as sources of atmospheric CO_2 . Deep-Sea. Res. II., 8: 578–590, 2009.

Clayton, T. D. and Byrne, R. H.: Spectrophotometric seawater pH measurements: total hydrogen ion concentration scale calibration of m-cresol purple and at-sea results. Deep-Sea. Res. I., 40(10): 2115–2129, 1993.

Cossarini, G., Lazzari, P., and Solidoro, C.: Spatiotemporal variability of alkalinity in the Mediterranean Sea. Biogeosci., 12: 1647–1658, 2015.

Cyronak, T., Santos, I.R., McMahon, A., Eyre, B.D.: Carbon cycling hysteresis in permeable carbonate sands over a diel cycle: Implications for ocean acidification. Limnol. Oceanogr., 58, 131-143, 2013.

Davison, W., Buffle, J., and DeVitre, R.: Voltammetric characterization of a dissolved iron sulphide species by laboratory and field studies. Anal. Chim. Acta, 377:193–203, 1998.

Davison, W.: The solubility of iron sulphides in synthetic and natural waters at ambient temperature. Aquat. Sci., 53(4): 309-329, 1991.

Dickson, A. G.: An exact definition of total alkalinity and a procedure for the estimation of alkalinity and total inorganic carbon from titration data. Deep-Sea. Res. A, 28 (6):609–623, 1981.

Dickson, A.G., Sabine, C.L., Christian, J.R.: Guide to best practices for ocean CO_2 measurements. In: Dickson, A.G., Sabine, C.L., Christian, J.R. (Eds.), PICES Special Publication. 3. pp. 191, 2007.

Estournel, C., Kondrachoff, V., Marsaleix, P., and Vehil, R.: The Plume of the Rhone: numerical simulation and remote sensing. Cont. Shelf. Res., 17(8):899–924, 1997.

Ferron, S., Alonso-Perez, F., Ortega, T. and Forja, J.M.: Benthic respiration on the northeastern shelf of the Gulf of Cádiz. Mar. Ecol. Prog. Ser., 392: 69-80, 2009.

Friedl, G., Dinkel, C., and Wehrli, B.: Benthic fluxes of nutrients in the northwestern Black Sea. Mar. Chem., 62:77–88, 1998.

Gaillard, J.-F., Pauwels, H., and Michard, G.: Chemical diagenesis in coastal marine sediments. Oceanol. Acta, 12(3):173–187, 1989.

Got, H. and Aloisi, J. C.: The Holocene sedimentation on the Gulf of Lions margin: a quantitative approach. Cont. Shelf. Res., 10(9-11):841–855, 1990.

Grasshof, K., Ehrhardt, M. and Kremling, K.: Methods of Seawater Analysis, second revised and extended edition. Verlag Chemie GmbH, 420 pp, 1983.

Hammond, D.E., Giordani, P., Berelson, W.M. and Poletti, R.: Diagenesis of carbon and nutrients and benthic exchange in sediments of the Northern Adriatic Sea. Mar. Chem., 66: 53-79, 1999.

Hartnett, H. E., Keil, R. G., Hedges, J. I., and Devol, A.: Influence of oxygen exposure time on organic carbon preservation in continental margin sediments. Nature, 391:572–575, 1998.

Hedges, J. I. and Keil, R. G.: Sedimentary organic matter preservation: an assessment and speculative synthesis. Mar. Chem., 49:81–115, 1995.

Henneke, E., Luther, G., and Delange, G.: Determination of inorganic Sulfur Speciation with Polarographic Techniques - some preliminary Results for Recent Hypersaline Anoxic Sediments. Mar. Geol., 100:115–123, 1991.

Hu, X. and Cai, W.-J.: An assessment of ocean margin anaerobic processes on oceanic alkalinity budget. Glob. Biogeochem. Cycl., 25:1–11, 2011a.

Hu, X. and Cai, W.-J.: The impact of denitrification on the atmospheric CO2 uptake potential of seawater. Mar. Chem., 127: 192-198, 2011b.

Jahnke, R. A. and Christiansen, M. B.: A free-vehicle benthic chamber instrument for sea floor studies. Deep-Sea. Res., 36(4): 625–637, 1989.

Jahnke, R. A.: A Global synthesis. In: Carbon and Nutrient Fluxes in Continental Margins, pages 597-615. K.-K. Liu, L. Atkinson, R. Quinones, L. Talaue-McManus (eds), Berlin, 2010.

Jones, M., Fennessey, C., DiChristina, T., and Taillefert, M.: Shewanella oneidensis MR-1 mutants selected for their inability to produce soluble organic-Fe(III) complexes are unable to respire Fe(III) as anaerobic electron acceptor. Envir. Microb., 12: 938–950, 2010.

Jørgensen, B. B. and Kasten, S.: Sulfur cycling and methane oxidation. In Marine Geochemistry. pp 271-310. Schulz H.D. et al. (eds), Springer Verlag, 2006.

Jourabchi, P., Van Cappellen, P., and Regnier, P.: Quantitative interpretation of pH distributions in aquatic sediments: A reaction-transport modeling approach. Amer. J. Sci., 305(9): 919–956, 2005.

Komada, T., Burdige, D. J., Li, H.-L., Magen, C., Chanton, J. P., and Cada, A. K.: Organic matter cycling across the sulfate-methane transition zone of the Santa Barbara Basin, California Borderland. Geochim. Cosmochim. Acta, 176: 259–278, 2016.

Krumins, V., Gehlen, M., Arndt, S., Van Cappellen, P., and Regnier, P.: Dissolved inorganic carbon and alkalinity fluxes from coastal marine sediments: model estimates for different shelf environments and sensitivity to global change. Biogeosci., 10(1): 371–398, 2013.

Lansard, B., Rabouille, C., Denis, L., and Grenz, C.: In situ oxygen uptake rates by coastal sediments under the influence of the Rhône River (NW Mediterranean Sea). Cont. Shelf. Res., 28(12): 1501–1510, 2008.

Lansard, B., Rabouille, C., Denis, L., and Grenz, C.: Benthic remineralization at the land–ocean interface: A case study of the Rhône River (NW Mediterranean Sea). Estuar. Coast. Shelf Sci., 81(4): 544–554, 2009.

Lehrter, J., Beddick, D., Devereux, R., Yates, D., and Murrel, M.: Sediment-water fluxes of dissolved inorganic carbon, O_2, nutrients, and N_2 from the hypoxic region of the Louisiana continental shelf. Biogeochem., 109 (1-3): 233–252, 2012.

Li, Y.-H. and Gregory, S.: Diffusion of ions in sea water and in deep-sea sediments. Geochim. Cosmochim. Acta, 38: 703–714, 1974.

Łukawska-Matuszewska, K. and Graca, B.: Pore water alkalinity below the permanent halocline in the Gdańsk Deep (Baltic Sea) - Concentration variability and benthic fluxes. Mar. Chem., 204: 49-61, 2018.

Luther, G. W. and Ferdelman, T.: Voltametric Characterization of Iron (II) Sulfide Complexes in Laboratory Solutions and in Marine Waters and Porewaters. Environ. Sci. Technol., 27: 1154–1163, 1993.

Luther, G. W., Glazer, B., Ma, S., Trouwborst, R., Moore, T., Metzger, E., Kraiya, C., Waite, T., Druschel, G., Sundby, B., Taillefert, M., Nuzzio, D., Shank, T., Lewis, B., and Brendel, P.: Use of voltammetric solid-state (micro)electrodes for studying biogeochemical processes: Laboratory measurements to real time measurements with an in situ electrochemical analyzer(ISEA). Mar. Chem., 108:221–235, 2008.

Maillet, G.M. Vella, C., Berné, S., Friend, P. L., Amos, C. L., Fleury, T. J. and Normand, A.: Morphological changes and sedimentary processes induced by the December 2003 flood event at the present mouth of the Grand Rhône River (southern France). Mar. Geol., 234(1): 159-177, 2006.

McKee, B. A., Aller, R. C., Allison, M. A., Bianchi, T. S., and Kineke, G. C.: Transport and transformation of dissolved and particulate materials on continental margins influenced by major rivers: benthic boundary layer and seabed processes. Cont. Shelf. Res., 24:899–926, 2004.

Millero, F.J. and Schreiber, D.R.: Use of the ion pairing model to estimate activity coefficients of the ionic components of natural waters. Am. J. Sci., 282: 1508-1540, 1982.

Millero, F.J.: The estimation of the pK^*_{HA} of acids in seawater using the Pitzer equations. Geochim. Cosmochim. Acta, 47: 2121-2129, 1983.

Millero, F. J.: Thermodynamics of the carbon dioxide system in the oceans. Geochim. Cosmochim. Acta, 59, 661–677, 1995.

Miralles, J., Radakovitch, O., and Aloisi, J.-C.: ^{210}Pb sedimentation rates from the Nothwestern Mediterranean margin. Mar. Geol., 216:155–167, 2005.

Mucci, A.: The solubility of calcite and aragonite in seawater at various salinities, temperatures and one atmosphere total pressure, Am. J. Sci., 283, 780–799, 1983.

Mucci, A., Sundby, B., Gehlen, M., Arakaki, T., Zhong, S., and Silverberg, N.: The fate of carbon in continental shelf sediments of eastern Canada: a case study. Deep S. Res. Part II: Topical Studies in Oceanography, 47:733–760, 2000.

Muller-Karger, F.E. et al. : The importance of continental margins in the global carbon cycle, Geophys. Res. Lett., 32, L01602, doi:10.1029/2004GL021346, 2005.

Murphy, J. and Riley, J. P.: A modified single solution method for determination of phosphate in natural waters. Anal. Chim. Acta, 27:31–36, 1962.

Nakayama, N., Tokieda, T., Suzuki, A., Kim, T., Gamo, T., and Obata, H.: Size fractionation of nanoparticulate metal sulfides in oxic water of Lake Teganuma, Japan. Geochem. J., 50:281–286, 2016.

Ortega, T., Ponce, R., Forja, J. and Gomez-Parra, A.: Benthic fluxes of dissolved inorganic carbon in the Tinto-Odiel system (SW of Spain). Cont. Shelf. Res., 28: 458-469, 2008.

Pastor, L., Cathalot, C., Deflandre, B., Viollier, E., Soetaert, E., Meysmann, K., Ulses, F. J. R., Metzger, C., and Rabouille, C.: Modeling biogeochemical processes in sediments from the Rhône River prodelta area (NW Mediterranean Sea). Biogeosci., 8:1351–1366, 2011.

Pyzik, A. and Sommer, S.: Sedimentary Iron Monosulfides - Kinetics and Mechanism of Formation. Geochim. Cosmochim. Acta, 45:687–698, 1981.

Rabouille, C., Mackenzie, F. T. and Ver, L. M.: Influence of the human perturbation on carbon, nitrogen, and oxygen biogeochemical cycles in the global coastal ocean. Geochim. Cosmochim. Acta 65: 3615-3641, 2001.

Rabouille, C., Denis, L., Dedieu, K., Stora, G., Lansard, B., and Grenz, C.: Oxygen demand in coastal marine sediments: comparing in situ microelectrodes and laboratory core incubations. J. Exp. Mar. Biol. Ecol., 285:49–69, 2003.

Radakovitch, O., Cherry, R., and Heussner, S.: ^{210}Pb and ^{210}Po: tracers of particle transfer on the Rhône continental margin (NW Mediterranean). Deep S. Res. Part I: Oceanogr. Res. Pap., 46(9):1539–1563, 1999.

Rao, A.M.F., Malkin, S.Y., Montserrat, F. and Meysman, F.J.R.: Alkalinity production in intertidal sands intensified by lugworm bioirrigation. Estuar. Coast. shelf Sci., 148, 36-47, 2014.

Rassmann, J., Lansard, B., Pozzato, L., and Rabouille, C.: Carbonate chemistry in sediment pore waters of the Rhône River delta driven by early diagenesis (NW Mediterranean). Biogeosci., 13(18): 5379–5394, 2016.

Rickard, D. and Luther, G. W.: Kinetics of pyrite formation by the H_2S oxidation of iron(II) monosulfide in aqueous solutions between 25 and 125 °C: the mechanism. Geochem. Cosmochem. Acta, 61:135–147, 1997.

Roussiez, V., Aloisi, J.-C., Monaco, A., and Ludwig, W.: Early muddy deposits along the Gulf of Lions shoreline: A key for a better understanding of land-to-sea transfer of sediments and associated pollutant fluxes. Mar. Geol., 222-223:345–358, 2005.

Rowe, G., Kaegi, M., Morse, J., Boland, G., and Briones, E.: Sediment community metabolism associated with continental shelf hypoxia, Northern Gulf of Mexico. Estuaries, 25: 1097–1106, 2002.

Rozan, T., Taillefert, M., Trouwborst, R., Glazer, B., Ma, S., Herszage, J., Valdes, L., Price, K., and Luther, G.: Iron-sulfur-phosphorus cycling in the sediments of a shallow coastal bay: Implications for sediment nutrient release and benthic macroalgal blooms. Limnol. Oceanogr., 47: 1346–1354, 2002.

Sarradin, P.-M. and Caprais, J.-C.: Analysis of dissolved gases by headspace sampling gas chromatography with column and detector switching. Preliminary results. Anal. Comm., 33:371–373, 1996.

Seeberg-Elverfeldt, J., Schlüter, M., Feseker, T., and Kölling, M.: Rhizon sampling of pore waters near the sediment/water interface of aquatic systems. Limnol. Oceanogr. Meth., 3:361–371, 2005.

Sempéré, R., Charrière, B., Wambeke, F. V., and Cauwet, G.: Carbon inputs of the Rhône River to the Mediterranean Sea: Biogeochemical implications. Glob. Biogeochem. Cycles, 14(2): 669–681, 2000.

Soetaert, K., Hofmann, A. F., Middelburg, J. J., Meysman, F. J. R., and Greenwood, J.: The effect of biogeochemical processes on pH. Mar. Chem., 105: 30–51, 2007.

Stookey, L.: Ferrozine - a new spectrophotometric reagent for iron. Anal. Chem., 42(7): 779–781, 1970.

Taillefert, M., Beckler, J., Carey, E., Burns, J., Fennessey, C., and DiChristina, T.: Shewanella putrefaciens produces an Fe(III)-solubilizing organic ligand during anaerobic respiration on insoluble Fe(III) oxides. J. Inorg. Biochem. 101: 1760–1767, 2007.

Taillefert, M., Bono, A. B., and Luther, G. W.: Reactivity of freshly formed Fe(III) in synthetic solutions and (pore)waters: Voltammetric evidence of an aging process. Environ. Sci. Technol., 34(11):2169–2177, 2000.

Taillefert, M., Hover, V. C., Rozan, T. F., Theberge, S. M., and Luther, G. W.: The influence of sulfides on soluble organic-Fe(III) in anoxic sediment porewaters. Estuaries, 25(6): 1088–1096, 2002.

Tercier-Waeber, M. and Taillefert, M.: Remote in situ voltammetric techniques to characterize the biogeochemical cycling of trace metals in aquatic systems. J. Environ. Monitor., 10:30–54, 2008.

Theberge, S.M. and Luther III, G.W.: Determination of the electrochemical properties of a soluble aqueous FeS species present in sulfidic solutions. Aquat. Geochem., 3: 191-211, 1997.

Thomas, H., Schiettecatte, L.-S., Suykens, K., Koné, Y. J. M., Shadwick, E. H., Prowe, A. E. F., Bozec, Y., de Baar, H. J., and Borges, A. V.: Enhanced ocean carbon storage from anaerobic alkalinity generation in coastal sediments. Biogeosci., 6(2):267–274, 2009.

Wolf-Gladrow, D. A., Zeebe, R. E., Klaas, C., Körtzinger, A., and Dickson, A. G.: Total alkalinity: The explicit conservative expression and its application to biogeochemical processes. Mar. Chem., 106:287–300, 2007.

Figure Captions

Figure 1: Map of the Rhône River prodelta with the stations investigated during the AMOR-B-Flux cruise in September 2015.

Figure 2: Dissolved oxygen and pH microprofiles recorded *in situ* at the sediment-water interface at stations A, Z, K, and E. Stations A and Z are located in the proximal zone, K in the prodelta, and E in the distal zone (i.e. continental shelf).

Figure 3: Temporal evolution of DIC and total alkalinity concentrations in the benthic chamber at stations A, Z (measured during two deployments), and E. Error bars represent analytical uncertainties determined from triplicate measurements. The benthic fluxes and their standard deviations are provided in the text, in Figure 4 and in Table 2.

Figure 4: DIC and TA fluxes measured with the benthic chamber and diffusive oxygen uptake (DOU) rates calculated from *in situ* microelectrode depth profiles at stations A, Z (measured during two deployments), and E. Error bars represent either uncertainties about the linear regression of the benthic DIC and TA gradients taking into account individual error bars of each data point or error propagation and standard deviations of multiple DOU measurements. Fluxes out of the sediment are positive and fluxes into the sediment are negative.

Figure 5: Depth profiles of dissolved O_2, Mn^{2+}, Fe^{2+}, org-Fe(III), FeS_{aq}, and ΣH_2S concentrations measured electrochemically in intact sediment cores at stations A, Z, AK, K, B, and E. Org-Fe(III) and FeS_{aq} are reported in normalized current intensities (nA).

Figure 6: Depth profiles of pore water TA, DIC, SO_4^{2-}, NH_4^+, CH_4, Ca^{2+}, nanoparticulate FeS (FeS_0), ΣPO_4^{3-}, and AVS concentrations along with the calcium carbonate (calcite) saturation state of the pore

waters (Ω_{Ca}) at stations A, Z, AK, K, B, and E. Alternating symbol shapes indicate data collected from duplicate long and short sediment cores. The calcium carbonate (calcite) saturation state (Ω_{Ca}) and pore water FeS_0 concentrations were calculated whereas AVS was determined from solid phase extractions. The two horizontal lines identify the sulfate-methane transition zone (SMTZ) found at stations A and Z. Error bars represent standard deviations of multiple measurements for the concentrations and error propagation for Ω. Concentrations of CH_4 were not measured at stations B, K, and E.

Figure 7: Current intensities of organic-Fe(III) complexes as a function of Fe^{2+} concentrations measured at each depth at stations A, Z, AK, B, and K compared to the same data obtained from iron-rich deep-sea sediments (Beckler et al., 2016).

Figure 8: Calculated pIAP values as a function of depth into the sediment compared to the pK_{sp} of amorphous FeS and mackinawite. Due to the lack of dissolved sulfide, the pIAP values in the pore waters of station A and Z could not be calculated.

Figure 9: Average pore water saturation states with respect to calcite in the oxic sediment layers at stations: a- Proximal (St. A, Z), b- prodelta (St. K), and c- distal (St. E) calculated using the DIC gradients at the SWI together with the average measured pH microprofiles.

Figure 10: Conceptual model to visualize the link between the burial of iron sulfide minerals and benthic alkalinity fluxes. The total alkalinity (TA) produced under anaerobic conditions at depth diffuses upwards towards the aerobic sediment layer where it is consumed during reoxidation of Fe^{2+} and ΣH_2S by dissolved oxygen (black). If the precipitation of sulfide minerals is significant, the reduced iron and sulfide metabolites produced during anaerobic respiration are not reoxidized by

dissolved oxygen, and the TA produced is able to reach the bottom waters (red). The intensity of the alkalinity flux into the bottom waters is indicated by the thickness of the arrow at the SWI.

Figure 11: TA to DIC benthic flux ratios as a function of depth at stations A, Z, and E of the Rhône River delta compared to different coastal regions of water depth < 100 m where this ratio was quantified from *in situ* benthic flux measurements (modified from Hu and Cai, 2011b). Other coastal regions include Cadiz Bay and the Guadalquivir continental shelf (Spain; Ferron et al., 2009), the Rio Tinto estuary (Spain; Ortega et al., 2008), the Po river delta and nearby Adriatic shelf (Italy; Hammond et al. 1999), San Francisco Bay (USA; Hammond et al., 1985), and the California shelf (USA; Berelson et al., 1996). The global coastal average TA to DIC flux ratio predicted from Krumins et al., 2013 is also reported for reference. Note that this average is different from that reported by Hu and Cai (2011b) which was corrected in their later publication (Hu and Cai, 2013).

Table captions

Table 1: Individual and consecutive microbial and abiotic reactions that affect the theoretical $\Delta TA/\Delta DIC$ (r_{AD}), $\Delta DIC/\Delta SO_4$ (r_{DS}), and $\Delta TA/\Delta sulfate$ (r_{AS}) stoichiometric ratios. Note that Eq. 14 and 17 include oxidation of H_2 produced by pyritization (Eq. 11) by sulfate-reducing bacteria.

Table 2: Sampling sites during the AMOR-B-Flux cruise in September 2015 and main characteristics of bottom waters; dist. = distance to the Rhône River mouth; ω = sedimentation rate; Station Z was sampled twice (Z on 09/08/15 and Z' on 09/14/15) to investigate temporal variability; n.d. = not determined.

Table 3: Diffusion-corrected stoichiometric ratios corrected (r_{ADc} , r_{DSc}, and r_{ASc}) or not (r_{AD}, r_{DS}, and r_{AS}) for carbonate precipitation along with their associated determination coefficients (r^2) from linear regression coefficients.

Biogeosciences Discuss., https://doi.org/10.5194/bg-2019-32
Manuscript under review for journal Biogeosciences
Discussion started: 4 February 2019

Table 4: Calculated FeS burial fluxes and their TA-equivalent production at each station compared to TA benthic fluxes measured; n.d. = not determined.

Biogeosciences Discuss., https://doi.org/10.5194/bg-2019-32
Manuscript under review for journal Biogeosciences
Discussion started: 4 February 2019

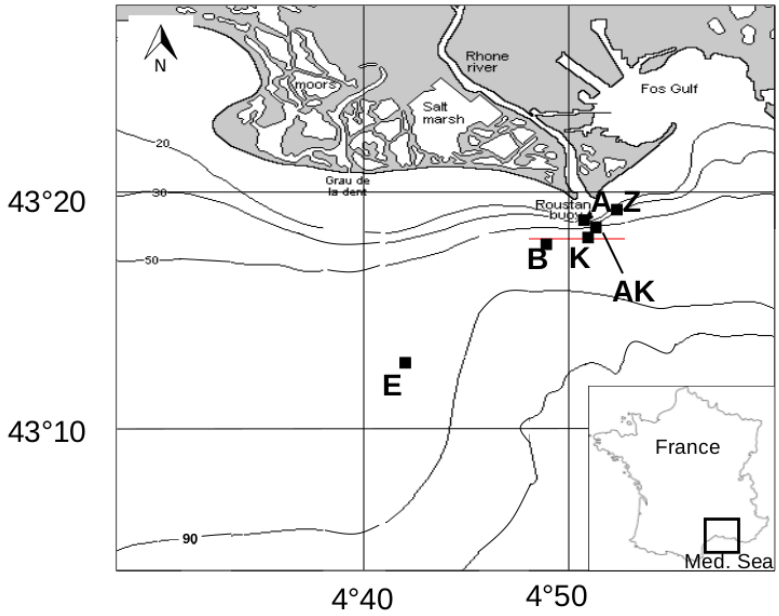

Figure 1: Figure 1

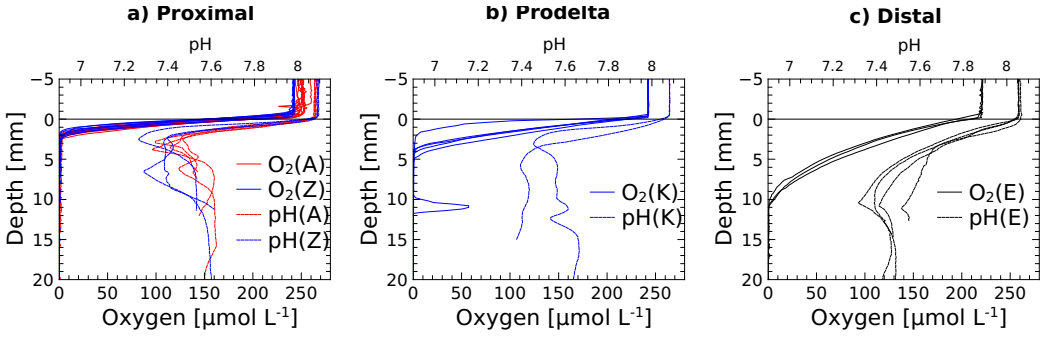

Figure 2: Figure 2

Biogeosciences Discuss., https://doi.org/10.5194/bg-2019-32
Manuscript under review for journal Biogeosciences
Discussion started: 4 February 2019

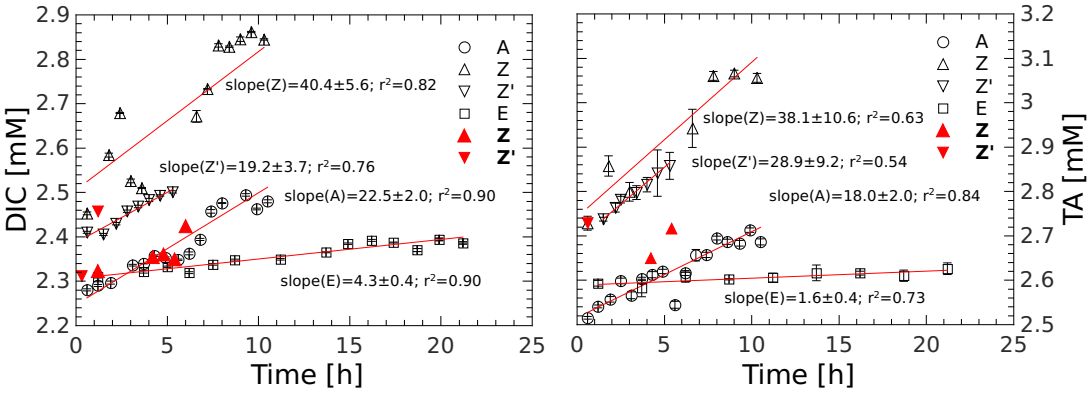

Figure 3: Figure 3

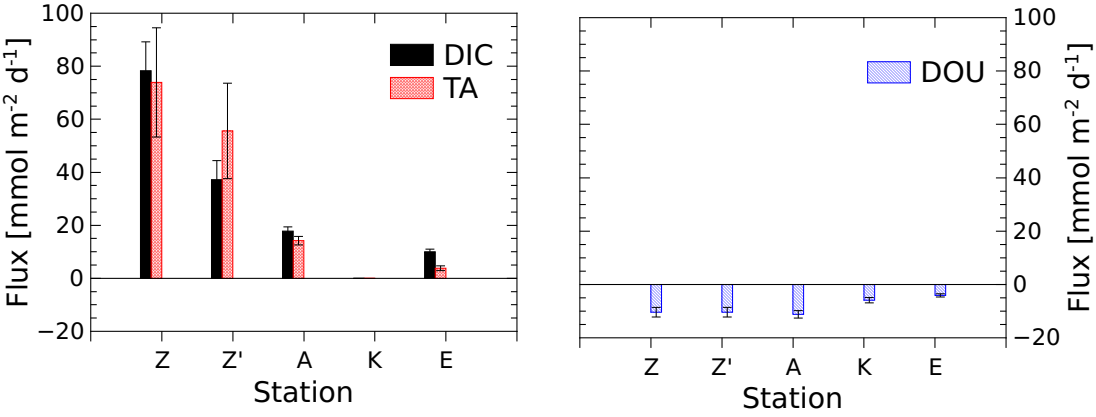

Figure 4: Figure 4

Biogeosciences Discuss., https://doi.org/10.5194/bg-2019-32
Manuscript under review for journal Biogeosciences
Discussion started: 4 February 2019

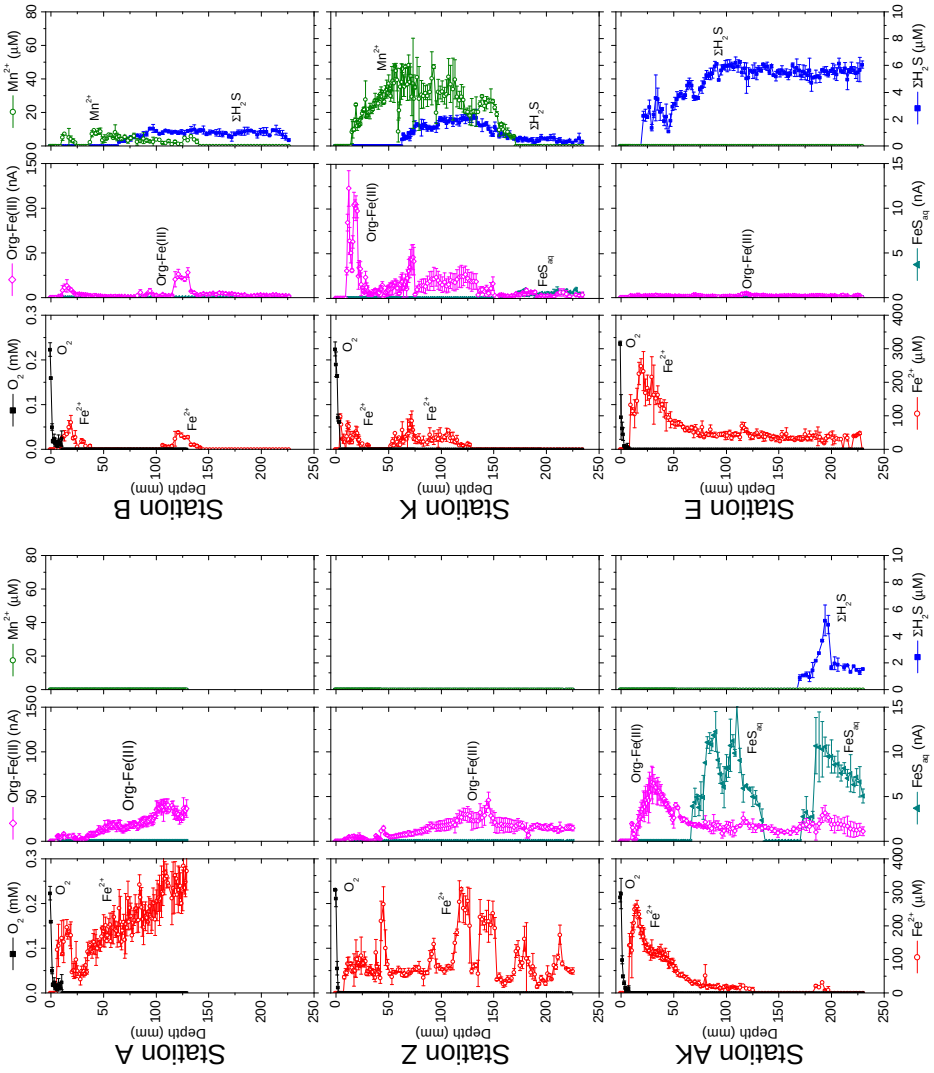

Figure 5: Figure 5

Biogeosciences Discuss., https://doi.org/10.5194/bg-2019-32
Manuscript under review for journal Biogeosciences
Discussion started: 4 February 2019

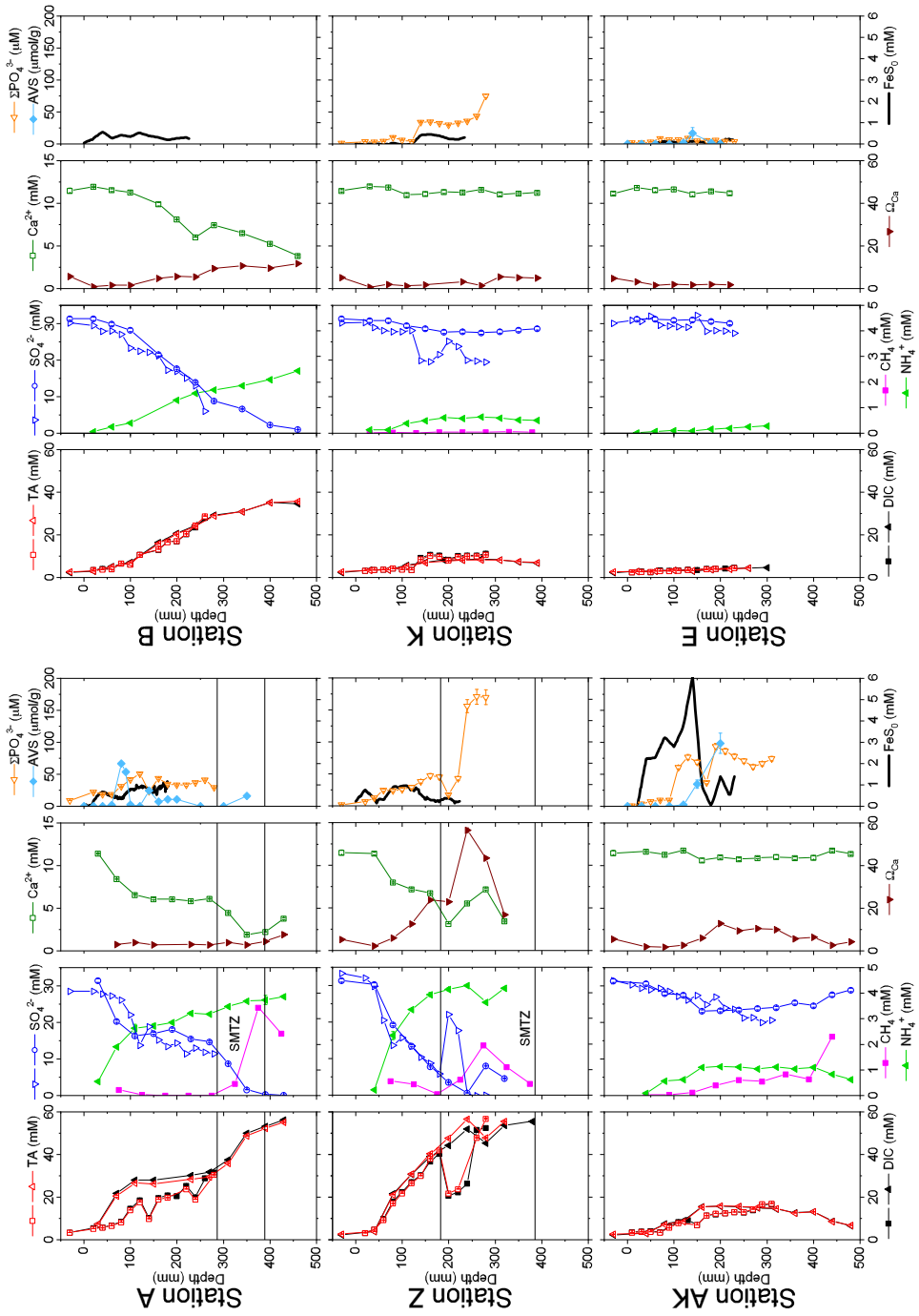

Figure 6: Figure6

Biogeosciences Discuss., https://doi.org/10.5194/bg-2019-32
Manuscript under review for journal Biogeosciences
Discussion started: 4 February 2019

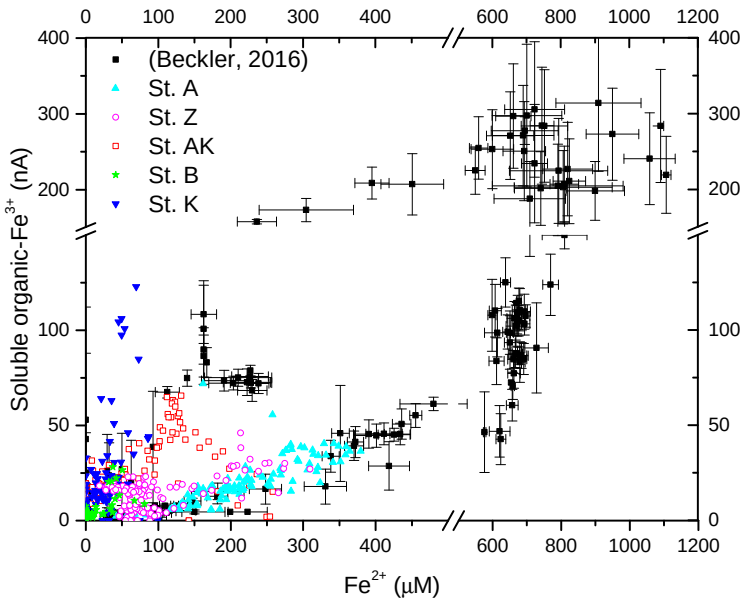

Figure 7: Figure 7

Biogeosciences Discuss., https://doi.org/10.5194/bg-2019-32
Manuscript under review for journal Biogeosciences
Discussion started: 4 February 2019

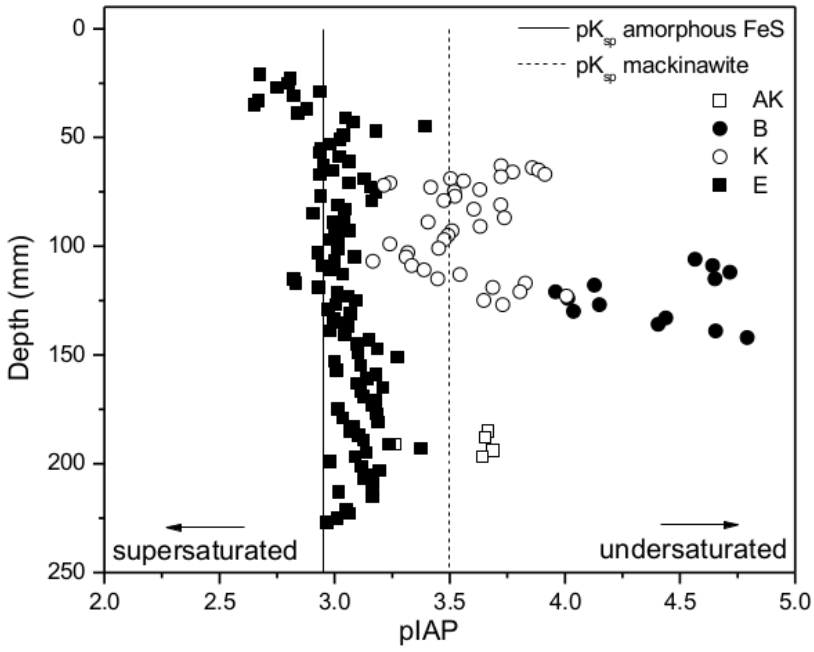

Figure 8: Figure 8

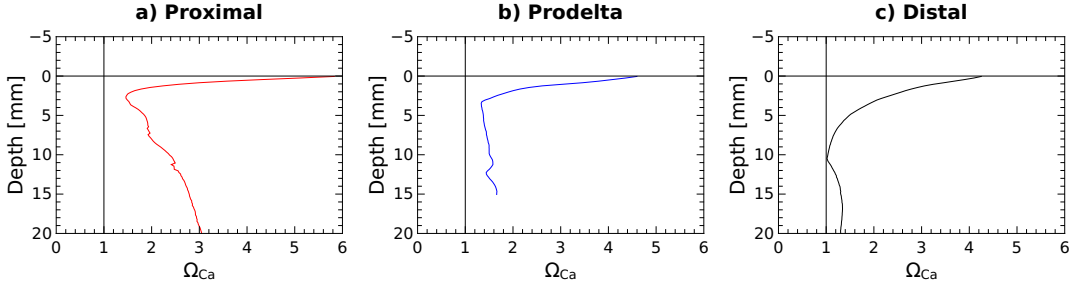

Figure 9: Figure 9

Biogeosciences Discuss., https://doi.org/10.5194/bg-2019-32
Manuscript under review for journal Biogeosciences
Discussion started: 4 February 2019

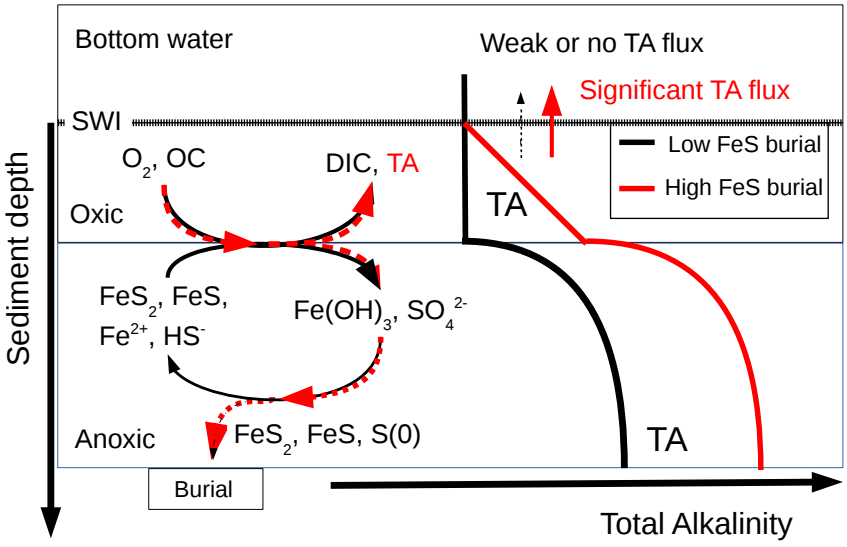

Figure 10: Figure 10

Biogeosciences Discuss., https://doi.org/10.5194/bg-2019-32
Manuscript under review for journal Biogeosciences
Discussion started: 4 February 2019

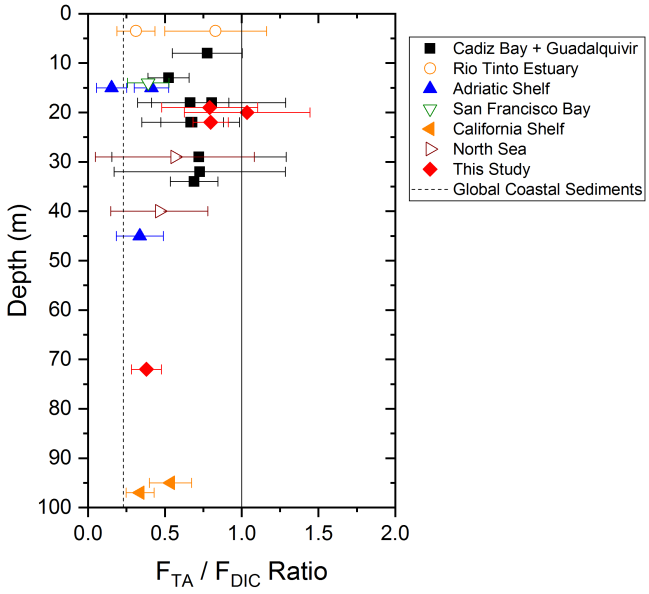

Figure 11: Figure 11

Biogeosciences Discuss., https://doi.org/10.5194/bg-2019-32
Manuscript under review for journal Biogeosciences
Discussion started: 4 February 2019

Table 1. Individual and consecutive microbial and abiotic reactions that affect the theoretical ΔTA/ΔDIC (r_{AD}), ΔDIC/Δsulfate (r_{DS}), and ΔTA/Δsulfate (r_{AS}) stoichiometric ratios. Note that Eq. 13 and 16 include oxidation of H_2 by sulfate reducing bacteria.

	Individual Reactions	r_{AD}	r_{DS}	r_{AS}
(1)	$Ca^{2+} + HCO_3^- \rightarrow CaCO_3 + H^+$	$\frac{-2}{-1} = 2$	-	-
(2)	$NH_4^+ + 2O_2 \rightarrow NO_3^- + 2H^+ + H_2O$	$\frac{-2}{0}$	-	-
(3)	$Fe^{2+} + \frac{1}{4}O_2 + \frac{5}{2}H_2O \rightarrow Fe(OH)_3 + 2H^+$	$\frac{-2}{0}$	-	-
(4)	$H_2S + 2O_2 \rightarrow SO_4^{2-} + 2H^+$	$\frac{-2}{0}$	-	$\frac{-2}{+1} = -2$
(5)	$CH_2O + \frac{4}{5}NO_3^- - \frac{2}{5}H^+ \rightarrow HCO_3^- + \frac{2}{5}N_2 + \frac{2}{5}H_2O$	$\frac{+4/5}{+1} = 0.8$	-	-
(6)	$2CH_2O + SO_4^{2-} \rightarrow 2HCO_3^- + H_2S$	$\frac{+2}{+2} = 1$	$\frac{+2}{-1} = -2$	$\frac{+2}{-1} = -2$
(7)	$CH_2O + 4\,Fe(OH)_3 + 7H^+ \rightarrow HCO_3^- + 4\,Fe^{2+} + 10\,H_2O$	$\frac{+8}{+1} = 8$	-	-
(8)	$CH_4 + SO_4^{2-} + H^+ \rightarrow HCO_3^- + H_2S + H_2O$	$\frac{+2}{+1} = 2$	$\frac{+1}{-1} = -1$	$\frac{+2}{-1} = -2$
(9)	$Fe(OH)_{3(s)} + \frac{1}{2}H_2S + 2H^+ \rightarrow Fe^{2+} + \frac{1}{2}S(0) + 3H_2O$	$\frac{+2}{0}$	-	-
(10)	$Fe^{2+} + H_2S \rightarrow FeS_{(s)} + 2H^+$	$\frac{-2}{0}$	-	-
(11)	$FeS_{(s)} + H_2S \rightarrow FeS_{2(s)} + H_2$	$\frac{0}{0}$	-	-
	Consecutive Reactions	r_{AD}	r_{DS}	r_{AS}
	Sulfate reduction, abiotic reduction of Fe(III) oxides, and precipitation of sulfide minerals			
(12)	$2CH_2O + SO_4^{2-} + \frac{2}{3}Fe(OH)_{3(s)} \rightarrow 2HCO_3^- + \frac{1}{3}S(0) + \frac{2}{3}FeS_{(s)} + 2H_2O$	$\frac{+2}{+2} = 1$	$\frac{+2}{-1} = -2$	$\frac{+2}{-1} = -2$
(13)	$2CH_2O + SO_4^{2-} + \frac{2}{5}Fe(OH)_{3(s)} \rightarrow 2HCO_3^- + \frac{1}{5}S(0) + \frac{2}{5}FeS_{2(s)} + \frac{6}{5}H_2O + \frac{2}{5}H_2$	$\frac{+2}{+2} = 1$	$\frac{+2}{-1} = -2$	$\frac{+2}{-1} = -2$
(14)	$\frac{20}{11}CH_2O + SO_4^{2-} + \frac{4}{11}Fe(OH)_{3(s)} + \frac{2}{11}H^+ \rightarrow \frac{20}{11}HCO_3^- + \frac{2}{11}S(0) + \frac{4}{11}FeS_{2(s)} + \frac{1}{11}H_2S + \frac{16}{11}H_2O$	$\frac{+2}{+20/11} = 1.1$	$\frac{+20/11}{-1} = -1.8$	$\frac{+2}{-1} = -2$
	Concomitant dissimilatory iron and sulfate reduction with precipitation of sulfide minerals			
(15)	$\frac{9}{4}CH_2O + SO_4^{2-} + Fe(OH)_{3(s)} \rightarrow \frac{9}{4}HCO_3^- + \frac{1}{4}H^+ + FeS_{(s)} + \frac{5}{2}H_2O$	$\frac{+2}{+9/4} = 0.89$	$\frac{+9/4}{-1} = -2.25$	$\frac{+2}{-1} = -2$
(16)	$\frac{17}{8}CH_2O + SO_4^{2-} + \frac{1}{2}Fe(OH)_{3(s)} \rightarrow \frac{17}{8}HCO_3^- + \frac{1}{8}H^+ + \frac{1}{2}FeS_{2(s)} + \frac{5}{4}H_2O + \frac{1}{2}H_2$	$\frac{+2}{+17/8} = 0.94$	$\frac{+17/8}{-1} = -2.13$	$\frac{+2}{-1} = -2$
(17)	$\frac{17}{9}CH_2O + SO_4^{2-} + \frac{4}{9}Fe(OH)_{3(s)} + \frac{1}{9}H^+ \rightarrow \frac{17}{9}HCO_3^- + \frac{4}{9}FeS_{2(s)} + \frac{1}{9}H_2S + \frac{14}{9}H_2O$	$\frac{+2}{+17/9} = 1.06$	$\frac{+17/9}{-1} = -1.89$	$\frac{+2}{-1} = -2$

Biogeosciences Discuss., https://doi.org/10.5194/bg-2019-32
Manuscript under review for journal Biogeosciences
Discussion started: 4 February 2019

Table 2. Sampling sites during the AMOR-B-Flux cruise in September 2015 and main characteristics of bottom waters; dist. = distance to the Rhône River mouth; ω = sedimentation rate; Station Z was sampled twice (Z on 09/08/15 and Z' on 09/14/15) to investigate temporal variability; n.d. = not determined.

Domain	**Proximal**			**Prodelta**			**Distal**
Stations	**A**	**Z**	**Z'**	**AK**	**B**	**K**	**E**
Long. ° E	4.850	4.868	4.868	4.853	4.833	4.858	4.684
Lat. °N	43.311	43.318	43.318	43.307	43.305	43.301	43.220
Dist. [km]	2.1	2.2	2.2	2.8	3	3.3	14.3
Depth [m]	20	20	20	42	50	58	72.5
Temp. [°C]	16.3	19.6	14.7	16.2	20.6	14.7	14.3
Salinity	37.5	37.6	37.7	37.7	38.0	37.7	37.8
O_2 [µM]	253.1 ± 0.3	249.5 ± 0.3	242.6 ± 0.2	250.2 ± 0.1	n.d.	241.8 ± 0.2	221.5 ± 0.3
DIC [mM]	2.29 ± 0.01	2.31 ± 0.01	n.d.	2.28 ± 0.01	2.27 ± 0.01	2.31 ± 0.01	2.33 ± 0.01
TA [mM]	2.61 ± 0.02	2.60 ± 0.01	n.d.	2.60 ± 0.02	2.60 ± 0.01	2.60 ± 0.02	2.61 ± 0.01
pH_T	8.08 ± 0.01	8.06 ± 0.01	8.09 ± 0.01	8.09 ± 0.01	8.07 ± 0.01	8.08 ± 0.01	8.05 ± 0.01
mean ϕ	0.69 ± 0.04	0.65 ± 0.04	0.65 ± 0.04	0.68 ± 0.02	0.66 ± 0.03	0.65 ± 0.05	0.64 ± 0.04
w [cm yr^{-1}]		30 - 40[a]			1 - 4[b]		0.1 - 1[c]
	Benthic fluxes (mmol m^{-2} d^{-1})						
TA flux	14.3 ± 1.6	73.9 ± 20.6	56.0 ± 17.8	n.d.	n.d.	n.d.	3.7 ± 0.9
DIC flux	17.8 ± 1.6	78.3 ± 10.9	37.2 ± 7.2	n.d.	n.d.	n.d.	9.9 ± 0.9
DOU	10.2 ± 1.3	10.4 ± 0.9	n.d.	n.d.	n.d.	5.9 ± 1.0	3.6 ± 0.6

a. Data from Charmasson et al., 1998
b. Data from Lansard et al., 2009
c. Data from Miralles et al., 2005

Biogeosciences Discuss., https://doi.org/10.5194/bg-2019-32
Manuscript under review for journal Biogeosciences
Discussion started: 4 February 2019

Table 3. Diffusion-corrected stoichiometric ratios r_{AD} , r_{DS}, and r_{AS} and their corresponding ratios corrected for carbonate precipitation (r_{ADc} , r_{DSc}, and r_{ASc}) along with their associated determination coefficients (r^2) from linear regression; n.d = not determined.

Stations	**A**	**Z**	**AK**	**B**	**K**	**E**
r_{AD}	0.99 ± 0.01	1.08 ± 0.02	1.02 ± 0.02	1.02 ± 0.01	0.98 ± 0.05	0.90 ± 0.04
r^2	0.998	0.997	0.998	0.999	0.986	0.984
r_{ADc}	1.10 ± 0.01	1.16 ± 0.03	1.07 ± 0.02	1.15 ± 0.02	1.06 ± 0.07	1.15 ± 0.11
r^2	0.999	0.997	0.996	0.998	0.974	0.885
r_{DS}	-1.67 ± 0.06	-1.87 ± 0.17	-1.85 ± 0.05	-1.18 ± 0.05	-1.72 ± 0.03	n.d.
r^2	0.990	0.969	0.995	0.988	0.997	n.d.
r_{DSc}	-1.88 ± 0.05	-2.05 ± 0.18	-1.95 ± 0.05	-1.37 ± 0.05	-1.86 ± 0.07	n.d.
r^2	0.994	0.972	0.996	0.990	0.994	n.d.
r_{AS}	-1.66 ± 0.07	-2.03 ± 0.17	-1.89 ± 0.06	-1.21 ± 0.04	-1.69 ± 0.07	n.d.
r^2	0.986	0.973	0.992	0.994	0.991	n.d.
r_{ASc}	-2.07 ± 0.05	-2.35 ± 0.14	-2.01 ± 0.06	-1.58 ± 0.05	-1.89 ± 0.14	n.d.
r^2	0.994	0.977	0.989	0.992	0.958	n.d.

Biogeosciences Discuss., https://doi.org/10.5194/bg-2019-32
Manuscript under review for journal Biogeosciences
Discussion started: 4 February 2019

Table 4. Calculated FeS burial fluxes and their TA-equivalent production at each station compared to alkalinity fluxes measured; n.d. = not determined.

Stations	**A and Z**	**AK**	**E**
ω [cm yr^{-1}]	30	3	0.1
ϕ	0.67	0.68	0.64
Mean [AVS] [µmol g^{-1}]	19.5 ± 4.9	45.0 ± 11.3	9.0 ± 2.3
sediment density [g cm^{-3}]	2.5	2.5	2.5
FeS burial flux [mmol S m^{-2} d^{-1}]	12.5 ± 3.8	4.9 ± 1.4	0.02 ± 0.01
TA-equivalent prod. (=2.0 FeS) [mmol TA m^{-2} d^{-1}]	25 ± 8	9.8 ± 2.8	0.04 ± 0.1
Measured TA flux at SWI [mmol TA m^{-2} d^{-1}]	A : 14.3 ± 1.6 Z : 73.9 ± 20.6 Z' : 56.0 ± 17.8	n.d.	3.7 ± 0.9